EUROPEAN ORGANIZATION FOR NUCLEAR RESEARCH

CERN-EP/88-171
November 30th, 1988

# MEASUREMENT OF $d\sigma/d\Omega$ AND $A_{on}$ IN $\bar{p}p$ ELASTIC SCATTERING BETWEEN 497 AND 1550 MEV/C

R.A.Kunne[1,*)], C.I.Beard[2,**)], R.Birsa[3)], K.Bos[1)], F.Bradamante[3)], D.V.Bugg[2)], A.S.Clough[4)], S.DallaTorre-Colautti[3)], J.A.Edgington[2)], J.R.Hall[2,***)], E.Heer[5)], R.Hess[5)], J.C.Kluyver[1)], C.Lechanoine-Leluc[5)], L.Linssen[1,**)], A.Martin[3)], T.O.Niinikoski[6)], Y.Onel[5,†)], A.Penzo[3)], D.Rapin[5)], J.M.Rieubland[6)], A.Rijllart[6)], P.Schiavon[3)], R.L.Shypit[4,††)], F.Tessarotto[3)], A.Villari[3)] and P.Wells[2)]

Abstract: Measurements have been made of the differential cross section and asymmetry $A_{on}$ for $\bar{p}p$ elastic scattering at 15 incident momenta between 497 MeV/c and 1550 MeV/c. The angular range where both particles have enough energy to traverse target and setup has been covered. The results are compared with predictions of various $\bar{N}N$ potential models. None of these models fully explains the present results, although the general trend of the data is predicted correctly.

---

1) NIKHEF-H, Amsterdam, The Netherlands
2) Queen Mary College, London, England
3) INFN Trieste and University of Trieste, Trieste, Italy
4) University of Surrey, Guildford, Surrey, England
5) DPNC, University of Geneva, Geneva, Switzerland
6) CERN, Geneva, Switzerland

*) Present address: DPNC, University of Geneva, Geneva, Switzerland
**) Present address: CERN, Geneva, Switzerland
***) Present address: BNL, Upton NY, USA
†) Present address: University of Iowa, Iowa City IA, USA
††) Present address: SLAC, Stanford CA, USA

## 1. Introduction

The available differential cross section measurements in $\bar{p}p$ elastic scattering at low energy have provoked the publication of many papers describing these data in terms of $\bar{N}N$ potential models. The real test of these models has to be found in the measurement of the various spin observables. This paper describes the first high statistics measurement of the asymmetry parameter $A_{on}$ (also known as the polarization), as well as the differential cross section at 15 values of incident $\bar{p}$ momentum between 497 MeV/c and 1550 MeV/c at those angles were both particles leave the setup. The experiment was performed at the Low Energy Antiproton Ring (LEAR) at CERN.

At these low energies, the antinucleon-nucleon ($\bar{N}N$) interactions may be described by $\bar{N}N$ potentials. Although the long range part of the real part of these potentials can be derived from the much better known NN potentials, our understanding of $\bar{N}N$ potentials is far from complete. The short range part and the imaginary potential are dominated by annihilation, which so far has eluded a complete description.

Some phenomenological $\bar{N}N$ potential models have been proposed [1] [2] [3] [4] [5]. These models introduce a number of free parameters which have been adjusted using (part of) the available $\bar{N}N$ scattering data. In order to examine and discriminate between these models, good quality data on the $\bar{N}N$ spin observables are needed.

The measurement of spin dependent observables is also useful to face the open problem of the existence of broad $\bar{N}N$ resonances. This task requires a phase shift analysis with spin observables as necessary input.

Precise data on the differential cross sections of $\bar{p}p$ elastic scattering are known down to $p_{lab}$ = 180 MeV/c. Below 2 GeV/c high statistics differential cross section data were reported by Eisenhandler et al. [6] above 690 MeV/c, Brückner et al. [7] between 180 and 600 MeV/c and Kageyama et al. [8] between 390 end 780 MeV/c. Except for the data from Brückner et al. all these measurements were done with conventional beams. Asymmetry data are virtually non-existent. At low momentum (about 700 MeV/c) two bubble chamber measurements exist, Ohsugi et al. [9] and Kimura et al. [10]. The data from Albrow et al. [11] cover the momentum range between 910 and 2000 MeV/c and are the most exhaustive, but suffer from poor statistics beyond the first diffraction minimum. It is here that our data are a pronounced improvement.

Measurements of other spin observables do not exist as yet.

## 2. Experimental apparatus

### *2.1 The setup*

The experiment [12] was carried out at the CERN Low Energy Antiproton Ring, using a polarized proton target. This target consisted of a 3 cm long cylinder with diameter 1 cm, which was filled with pentanol at 0.5 K. The target length was 1.94 g/cm$^2$ corresponding to a hydrogen length of 0.264 g/cm$^2$. The proton polarization, typically 75%, was reversed every few hours. The target was placed in a locally homogeneous magnetic field of 25 kG, provided by a C−shaped dipole magnet. The total bending power of this field was 4.2 kGm. The background caused by scatterings on protons bound in carbon and oxygen, was calculated from runs with a dummy target containing teflon. The experiment was designed to measure the three twobody reactions $\bar{p}p \rightarrow \bar{p}p$, $\bar{p}p \rightarrow \pi^-\pi^+$ and $\bar{p}p \rightarrow K^-K^+$. The scattered and recoil particles were detected in the angular range were both proton and antiproton had enough energy to traverse target and setup. This acceptance increased from $-.28 < \cos\theta_{cm} < .28$ at 497 MeV/c to $-.84 < \cos\theta_{cm} < .80$ at 1550 MeV/c. Proton and antiproton were detected in three multiwire proportional chambers (see figure 1). Immediately around the target, but still in the gap of

the magnet, were a J-shaped and a C-shaped MWPC, with two planes of vertical wires each. The J-chamber had one plane of cathode strip read out, mounted at an angle of 30° with the horizontal plane. Further out were two MWPCs, one on the left and one on the right of the outgoing beam. These chambers also had two planes of vertical wires and two planes of cathode strips. read out to provide information about the polar scattering angle $\phi_{cm}$. The L-chamber had a width of 92°. Depending on the deflection of the beam, the R-chamber used, was either 152° or 171° wide. An array of overlapping trigger scintillators was placed around this setup, split in the same way as the outer chambers. Both the outer chambers and the trigger scintillators could rotate around the magnet on rails. This arrangement allowed to change the detector positions, as the deflection of the beam changed with momentum.

The incoming beam track was reconstructed from the information provided by the J- and C-chamber as well as by two beam chambers made of low density materials. Each beam chambers had one plane of horizontal wires and one plane of vertical wires.

### *2.2 The twobody trigger*

The beam trigger consisted of a triple beam counter coincidence B0.S1.S2 or B0.S1.S3. B0 was placed 24 m upstream of the target, S1 44 cm upstream, just inside the outer chamber. S2 and S3 were scintillators of diameter 10 mm and 7 mm respectively directly in front of the target. They were aligned on the target to better than 1 mm horizontally, and 2 mm vertically, by scans that measured the transmission of $\bar{p}$s through the target. Horizontally mounted close to the pole faces of the magnet were two veto counters (not shown in figure 1) to reject events with particles going outside the acceptance of the chambers. The trigger for the twobody reactions required exactly one particle in the L-scintillator array and exactly one in the R-sector, having approximately the correct kinematics. This trigger initiated the MWPC read out. Using the information from the scintillators and the outer MWPCs, the kinematical constraint was tightened. At this second trigger level it was already possible to distinguish between elastic events on the one hand and $\pi^-\pi^+$ and $K^-K^+$ events on the other hand. A filter using information from the C- and the R-chamber rejected events that were obvious annihilations in the C-chamber outgoing beam region. The candidate events, 60 per second at a typical beam rate of 300K per second, were written to tape for further analysis.

### *2.3 The two event topologies*

The collection of elastic events fell apart in two event topologies. The events with the forward scattered antiproton going to the left and with azimuthal angle $\phi_{cm}$ around 0° will be denoted as PM. The events with the recoil proton going to the left and with $\phi_{cm}$ around 180° will be denoted as PP. Acceptance and background for the two event topologies were not the same, mainly due to the different effect of the presence of the magnetic field. In the analysis they were handled separately.

## 3. Analysis

### *3.1 The matrix reconstruction method*

The events were reconstructed with the use of a matrix method. The formalism of the reconstruction is based on the method described in [13]. It was successfully used in an experiment by the Geneva group at SIN [14].

The kinematics of a twobody event can be fully described with seven parameters. In our experiment these were the three vertex coordinates $v_x$, $v_y$ and $v_z$, the polar and azimuthal scattering angles in the center of mass frame $\theta_{cm}$ and $\phi_{cm}$ and the vertical and horizontal incidence angles of the incoming

particle $\alpha_v$ and $\alpha_h$. Together they form the parameter vector $\vec{p}$. To each event given by $\vec{p} = (v_x, v_y, v_z, \theta_{cm}, \phi_{cm}, \alpha_v, \alpha_h)$ corresponds an unique vector of MWPC hits $\vec{x}$ (also called coordinate vector).

The relation between $\vec{p}$ and $\vec{x}$ is given by a function, depending on the parameters of the setup, the 'design equation':

$$\vec{x} = \vec{f}(\vec{p})$$

A reconstruction program inverts this function $\vec{f}$ and calculates $\vec{p}$ from $\vec{x}$. If one defines a central parameter vector $\vec{p}_0$, corresponding to a central coordinate vector $\vec{x}_0$, the design equation can be expressed as a Taylor expansion:

$$\vec{x} = \vec{f}(\vec{p}_0) + \left(\frac{\partial \vec{f}}{\partial \vec{p}}\right)_{(\vec{p}=\vec{p}_0)} \cdot (\vec{p}-\vec{p}_0) + \text{higher order terms}$$

$$= \vec{x}_0 + \tilde{D}\,(\vec{p}-\vec{p}_0) + \text{higher order terms}$$

$\tilde{D}$ is called the design matrix and can be calculated, by simulating twobody events with parameter vectors at a small distance $\partial\vec{p}$ from the central parameter.

If the parameter vector $\vec{p}$ is close to the central parameter vector, it is permitted to ignore the higher order terms in the expansion. The coordinate vector $\vec{x}$ then is a linear function of $\vec{p}$. By inverting this linear equation, it is possible to express $\vec{p}$ as a linear function of $\vec{x}$:

$$\vec{p} = \vec{p}_0 + \tilde{R}\,(\vec{x}-\vec{x}_0)$$

where $\tilde{R}$ is called the reconstruction matrix. In order to invert $\tilde{D}$ to find this matrix $\tilde{R}$, one also needs the covariance matrix $\tilde{C}$ of the measured coordinates, or rather its inverse $\tilde{G}$, the weight matrix. The matrix $\tilde{G}$ can be calculated by looking at the effects of all possible error sources on the coordinates in the MWPCs. Once $\tilde{G}$ is known, the reconstruction matrix follows:

$$\tilde{R} = (\tilde{D}^{\dagger}\,\tilde{G}\,D)^{-1}\,\tilde{D}^{\dagger}\,\tilde{G}$$

where $\tilde{D}^{\dagger}$ is the design-matrix transposed. The $\chi^2$ of the solution is calculated in the following way:

$$\chi^2 = \vec{s}^{\dagger}\,\vec{s}$$

where s is called the residue vector, given by:

$$\vec{s} = \tilde{Y}\,(\vec{x}-\vec{x}_0) \quad \text{with} \quad \tilde{Y} = \tilde{B}\,(\tilde{I} - \tilde{D}\,\tilde{R})$$

and $\tilde{B}$ is given by $\tilde{G} = \tilde{B}^{\dagger}\,\tilde{B}$.

The formalism described so far would be complete if the higher order terms of the design equation really can be ignored. This is permitted only if the magnitude of the non-linearities is small compared to the errors in the measured coordinate vector. But in general this is not the case: the ranges of the parameters, which are accepted by the setup, are large and the non-linearities in the Taylor expansion grow rapidly, when one leaves the vicinity of the central parameter vector. The Monte Carlo program that calculated the matrices, showed that the non-linearities are non-negligible only for three of the seven parameters: $v_z$, $\theta_{cm}$ and $\phi_{cm}$. The higher order terms of the other four parameters were small enough to be ignored. Therefore for each matrix a three dimensional table was calculated, containing the corrections for the non-linearities.

The advantage of the method described is speed in reconstruction. By dividing the angular ranges of the three twobody reactions in pieces with a width of the order of 6° the non−linearity corrections never grew larger than 10 mm and depending on momentum up to 42 matrices were needed.

### *3.2 Event selection*

The kinematical reconstruction program described above selected events with $\chi^2$/DF for at least one of the three reactions less than 30. This reduced the data sample typically by a factor three or four to about 500K events per momentum, of which 90% were elastic event candidates and 10% mesons. To reduce the number of elastic data further, different cuts were made to obtain an asymmetry data sample and a differential cross section data sample. For the asymmetry data sample we imposed the criteria:

1. A vertex cut of $|v_z| < 12$ mm, where $v_z$ is the longitudinal coordinate in the target.
2. A trigger given by S2, the bigger of the two target scintillators.
3. An azimuthal angle cut of $|\phi_{cm}| < 15°$.

For the cross section data sample the cuts were tightened to ensure a correct calculation of efficiency and geometrical acceptance:

1. A vertex cut of $|v_z| < 12$ mm, where $v_z$ is the longitudinal coordinate in the target.
2. A trigger given by S3, the smaller of the two target scintillators.
3. An azimuthal angle cut of $|\phi_{cm}| < 6°$.

The third cut was dictated by the fact that the acceptance of the setup was limited in $\phi_{cm}$ by the height of the hodoscope counters and MWPCs. As no accurate vertical information was available in the J- and C-chamber, it was decided to make this cut safely inside the region where the acceptance was likely to drop. The obvious price to pay when adopting this method was a drastic loss in statistics of about a factor two.

### *3.3 Background subtraction*

The $\chi^2$ distribution of the events at one momentum is shown in figure 2. The large tail is entirely due to quasi-elastic events and may be extrapolated to low values of $\chi^2$ to give the amount of background under the signal. The shape of the background distribution was measured collecting data with the dummy target. The events from these runs were reconstructed and selected in exactly the same way as the pentanol target data. As the amount of background depended on $\theta_{cm}$, the normalization was done separately for each $\cos\theta_{cm}$ bin.

This normalization turned out to be not very sensitive to the exact definition of the tail. Normalization with the cuts varying from $8 \leq \chi^2/DF \leq 15$ led to results that were identical within errors both for asymmetry and differential cross sections. The dummy target runs were taken only at three momenta (523, 1089 and 1434 MeV/c) which each have rather different acceptances. For the intermediary runs the background shape was determined by linear interpolation between the two closest momenta. The shape of the $\chi^2$/DF distribution varied only little with momentum. This was checked by recalculating the background subtraction for each data set, using only the dummy target run that is in momentum closest to that set. The results were almost identical within the statistical errors.

### *3.4 Corrections applied to the data*

Most corrections that are necessary for the differential cross section calculation, are not needed for the asymmetry calculation, as they are the same for the two target polarizations.

The efficiency calculation was done separately for the events from the two target polarizations and the two event topologies (figure 3). The efficiency was calculated from the tracks found in the raw data sample. At most momenta it was not necessary to correct the asymmetry data for the inefficiency of the chambers, as the efficiency of the wire chambers was constant or drifted only slowly during the whole run. This was not the case for the two lowest momenta, 497 and 523 MeV/c, and therefore the asymmetry data for these momenta were corrected for inefficiency of the chambers.

A second cause of loss of events was due to the fact that the proton or antiproton did not always reach the hodoscope counters, but had an interaction somewhere in the target or setup. This absorption of secondaries increased with decreasing momentum of the particles, as the cross sections involved rise at lower energy. A Monte Carlo program was used to calculate this effect. The $\bar{p}$-nucleus and p-nucleus cross sections necessary for this simulation were obtained from [15] and [16] respectively. The former was fitted by a function of the form $( c_1 + c_2 A^{1/3} )^2$, where A is the atomic number of the nucleus and $c_1$ and $c_2$ are both of the form $A_i + B_i p + C_i / p$ (p momentum), as was suggested by [17].

In the case of p-nucleus the data points between $A = 4$ and $A = 64$ were fitted to a 15 parameter function, which gave the cross sections at intermediate values.

Small corrections were needed to account for the absorption of the beam in the target, for random coincidences in the counters and for the effective length of the target as seen by the beam.

Table 1 gives a summary of the corrections applied to the differential cross section data. All corrections were calculated for each momentum separately.

### *3.5 Systematic errors*

The following systematic errors were dominant:

1. It is difficult to prove, whether the beam really did go through the full length of the target. Counter S3, which was smaller than the diameter of the target cylinder, was adjusted horizontally before each run, in such a manner that the number of antiprotons leaving the target was minimized. For momenta larger than 1000 MeV/c the beam spot was pencillike. At lower momenta the beam did blow up due to multiple scattering and filled S2, the larger of the two target counters, completely. Although the adjustment of S3 was done at every momentum, there was no guarantee that all the beam passing through S3, also traversed the whole target. Vertically the uncertainty might have been even bigger, due to the poor resolution in the reconstruction of the height of the vertex. An offset of only 1.5 mm of the centre of the counter from the centre of the target, would lose beam. The beam was scanned vertically, using a small vertical deflection magnet, and it was demonstrated that the centre of the target coincided with the centre of S3 within $\pm 2$ mm. However, the vertical image of the beam was larger than the horizontal one, since the final quadrupole was horizontally focussing. Assuming the counter never had an offset of more than 2.5 mm this systematic error was estimated to be $+6\%$.

2. The density of the target varied from run to run. This was due to a difference in packing fraction of the pentanol beads. This variation led to the suspicion that the target was not filled in a homogeneous way, but contained more pentanol in the lower part than in the higher part of the target. From the variation in the measured density and the difference in packing fraction the error was estimated to be $\pm 8\%$.

3. Systematic errors were caused by the uncertainties in the calculation of the absorption of secondary particles. These were mainly caused by the errors on the available p-nucleus and $\bar{p}$-nucleus cross sections. This error was estimated to be $\pm 2\%$.

4. In the Monte Carlo calculation of the absorption the loss due to straggling was underestimated. The Lorentzian tail of the straggling distribution was neglected. Instead the data points that needed a correction larger than 20% were discarded. The error on the surviving data points was estimated to be $+2\%$.

5. The error on the efficiency calculation was estimated to be $\pm 2\%$.

6. The dummy target measurement was done at only three momenta. As the shape of the $\chi^2$ distribution was slightly momentum dependent, a systematic error was introduced in the number of events subtracted. This error was estimated to be $\pm 2\%$.

7. The absolute calibration of the polarization of the pentanol target was $\pm 4\%$.

Only the last two errors had an influence on the asymmetry. The dominant systematic errors are summarized in table 2.

## 4. Results and discussion

### *4.1 Experimental results*

The experimental results on differential cross sections are presented in figures 4 till 11, together with our asymmetry data, which were already published in [18]. Numerical values may be found in Appendix A. The statistics of the differential cross section data are comparable with those of Eisenhandler et al. [6] and Kageyama et al. [8]. We believe the shape of $d\sigma/d\Omega$ to be entirely reliable. However, absolute normalization obtained using a polarized target is likely to be less reliable, than that obtained with a liquid hydrogen target. The data were normalized using a procedure described in the next section. In figure 12 the data at 783 MeV/c and 1089 MeV/c are compared with the data of Kageyama et al. and Eisenhandler et al. In the lower momentum of the two, the difference between the Eisenhandler data and our data stems entirely from a different normalization. In the backward direction the two previous experiments disagree. At 1089 MeV/c we agree with Eisenhandler et al. on the value of the forward point, but disagree by a factor 1.5 in the backward region. This momentum is the worst case. At all momenta however, our data are lower than the Eisenhandler et al. data. At some momenta the absolute value of the cross section is 10 to 20 percent smaller than the former.

At all momenta, $A_{on}$ tends to have two basic features: a broad positive asymmetry $\approx 0.4 \sin\theta_{cm}$, with rapid variations around the diffraction minima of $d\sigma/d\Omega$.

### *4.2 Legendre polynomial fits and normalization*

In a model independent way the differential cross section and asymmetry data can be expanded in orthogonal Legendre polynomials $P_\ell(\cos\theta)$ and $P^1{}_\ell(\cos\theta)$.

$$\frac{d\sigma}{d\Omega}(\cos\theta) = \sum_{\ell=0}^{L} a_\ell \, P_\ell(\cos\theta)$$

$$A_{on} \frac{d\sigma}{d\Omega}(\cos\theta) = \sum_{\ell=1}^{L} b_\ell \, P^1{}_\ell(\cos\theta)$$

The total elastic cross section $\sigma_{el}$ is equal to $4\pi a_0$. The coefficients $a_\ell/a_0$ and $b_\ell/a_0$ define the shape of the distributions and are adjusted to fit the data. The angular range of our data is limited: at 1550 MeV/c only 4% of the total elastic cross section is actually seen. Consequently the results for $\sigma_{el}$ have to be approached with due reserve.

The limited acceptance forced us to use extra constraints for the $d\sigma/d\Omega$ fits. These constraints also provided an absolute normalization of the data. As extra constraints on the Legendre expansion the forward differential elastic cross section $d\sigma(\theta = 0°)/d\Omega$ and its derivative were chosen. Extrapolating the fitted Legendre expansion to zero angle gives the elastic differential cross section at $\theta = 0°$. After correct normalization the extrapolated forward differential cross section must be equal to the forward scattering amplitude F(0) squared:

$$\frac{d\sigma(\theta = 0)}{d\Omega} = |F(0)|^2$$

If one neglects spin dependent amplitudes, the forward elastic cross section may be expressed in terms of ratio of real and imaginary parts of the forward scattering amplitude $\rho$ and the total cross section $\sigma_{tot}$. Using the optical theorem one may write

$$\frac{d\sigma(\theta = 0)}{d\Omega} = .1606\,(1 + \rho^2)\ \frac{k^2}{\pi^2}\ \sigma^2_{tot}$$

where the value of the constant is fixed when $d\sigma(\theta = 0)/d\Omega$ is given in mb/sr, c.m. momentum k in GeV/c and $\sigma_{tot}$ in mb.

To calculate $\rho$ and $\sigma_{tot}$ the data sets listed in tables 3 and 4 were used. In the case of the $\rho$ parametrization those data were chosen that correspond to fits with neglected spin-dependence parameter $\eta$. Taking $\eta$ non-zero and the corresponding $\rho$, changes the calculated value for the forward cross section less than a percent. This is not surprising as $\sigma_{tot}$, $\rho$ and $\eta$ are strongly correlated. The $\rho$ fit for $\eta = 0$ gave the result:

$$\rho = 0.245\,p^2 - 1.35\,p + 2.19 - 0.774\,/\,p \qquad [p \text{ in GeV/c}]$$

The several $\sigma_{tot}$ data sets do not have the same absolute normalization. Therefore in the fit, each set was given a normalization parameter, which was allowed to vary between .95 and 1.05. The parametrization became ($\sigma_{tot}$ in mb):

$$\sigma_{tot} = 64.3 + 53.8\,/\,p - 0.308\,/\,p^2 + 0.039\,/\,p^3 \qquad [p \text{ in GeV/c}]$$

The procedure described so far is similar to the one used by Coupland et al. [19], to extract the total elastic cross section from the elastic differential cross section data of Eisenhandler et al. [6]. The two results obtained for the forward nuclear cross section are shown in figure 13. They differ slightly as only the data set of Abrams et al. [20] was available in 1977. From the differences between the total cross section data samples used in the parametrization (see table 3), the error on the calculated forward point due to the uncertainties in the normalization of the total cross section and in $\rho$ is estimated to be $\pm 5\%$.

The second constraint was found in the derivative of the differential cross section at $\theta = 0°$. Close to zero the nuclear part of the differential cross section may be written as

$$\frac{d\sigma}{d\Omega} = \frac{d\sigma(\theta=0)}{d\Omega} \exp(-b\, q^2)$$

where $q^2$ is the momentum transfer squared $2k^2$ $(1 - \cos\theta)$ and b is the slope of the forward nuclear scattering amplitude. b (in $GeV^{-2}/c^{-2}$) is parametrized by Iwasaki et al. [21] as

$$b = 65.62 - 129.4\, p + 109.0\, p^2 - 30.19\, p^3 \qquad [p \text{ in GeV/c}]$$

The two extra constraints fixed the absolute normalization of the data. The normalization factors found in the procedure are shown in figure 14. They are consistent with one, although a decreasing trend with increasing momentum may be seen.

The fits to $d\sigma/d\Omega$ are done simultaneously with the fits to the asymmetry data. Results are shown in figures 15 and 16. and numerically in Appendix B.

A separate fit to the $d\sigma/d\Omega$ data changed the result only slightly. In table 5 the result of the complete fit and the separate fit are compared with the result of Eisenhandler et al. at 1090 MeV/c [6]. In the latter case both the numbers given in the reference and the result of the fit to their data using our procedure are presented. The fit to the Eisenhandler data with our normalization procedure was restricted to the same region of acceptance as our own data. Even so, the result of this fit and the fit of ref. [6] are consistent for the lower order coefficients. At higher order ($i > 4$) the differences are bigger, due to the fact that these coefficients are more sensitive to the derivative of the forward point. The same remark can be made for the comparison of our data with [6]: at higher order the values of the coefficients are markedly different. On top of that the overall normalization (given by $a_0$) differs 10-20%. This unexplained difference in the total elastic cross section appears for all measured momenta, as will be detailed in a later section.

For all data sets the fits were done with 7 to 16 Legendre coefficients. The fits for which the $\chi^2$ per degree of freedom reached a plateau were selected as final result. The number of coefficients necessary to represent the data becomes larger with momentum, up to twelve at 1550 MeV/c. Below 800 MeV/c only the coefficients $a_1$ till $a_6$ are important. In the procedure used, the higher order coefficients are determined mainly by the slope b.

In figures 17 and 18 (and Appendix B) the coefficients $b_i/a_0$, that determine the shape of the asymmetry data are given. It is difficult to give an interpretation for these results. The bumps at 783 and 1190 MeV/c are not due to differences of these momenta in the shape of the asymmetry distribution compared to their neighbours, but to different $d\sigma/d\Omega$ distributions. In fact the correlations between the $b_i$ and $a_j$ coefficients are large.

4.2.1 The total elastic cross section

From the Legendre fits follows the total elastic cross section. The latter is shown in figure 19 and compared with the results of Coupland et al. [19] and Kageyama et al. [8]. Our results turned out to be lower than [19], but agree with the two highest points of [8]. Numerical values are given in table 6. It is clear that the result is strongly correlated to the assumed values for the two constraints $d\sigma(\theta=0)/d\Omega$ and b.

The data put forward no additional evidence for the T resonance. This structure has been claimed by several experiments [19] [28] in the mass region of 2150-2200 $MeV/c^2$ (corresponding to a momentum of 1200-1350 MeV/c).

### *4.3 Comparison with potential models*

NN-potential models, based on meson exchanges to describe the long and medium range potential and complemented with a phenomenological short range potential, have been very successful in explaining the available NN scattering data, which form at certain energies a complete set.

Considering only meson exchange diagrams the $\bar{N}N$ and NN are related by the G-parity transformation. Recent models based on transformed NN potentials (of which the Bryan-Phillips potential [1] was the first) are for example the Dover-Richard model [2], the Paris model [3], the Bonn model [4] and the Nijmegen model [5].

All these models claim validity only below 900 MeV/c. They were developed at a time when only four asymmetry data points (at 700 MeV/c) were available: the data from the bubble chamber experiment of Kimura et al. [10] (see figure 20).

All potential models considered explain the gross features of the data. The shape of the differential cross section is faithfully reproduced by the models, at least in the forward angular region. The position of the diffraction minimum agrees. The differences between the models are most pronounced in their predictions for the asymmetry. The predictions of the four models for the asymmetries at 679 MeV/c are shown in figure 21 together with our data. All models succeed in predicting the position of the first maximum ($\cos\theta_{cm}\approx 0.5$) and the central minimum in $A_{on}$. The depth of the central minimum is always too pronounced. Most models predict large negative asymmetries that are not seen. Especially in the momentum range from 1000 till 1500 the central minimum is rather shallow with an asymmetry of 0.2-0.3.

The Paris model is the only one for which it is possible to extrapolate over the whole energy range of our experiment. The general trend of the $A_{on}$ data is foreseen nicely (figure 22). The model disagrees slightly on the magnitude of the asymmetry and especially on the depth of the central minimum. (figure 23)

### *4.4 Conclusion*

The availability of clean, intense antiproton beams at LEAR allows a considerable improvement in results of all antiproton experiments. The $A_{on}$ data in $\bar{p}p$ elastic scattering presented in this paper have statistical errors which are a factor five to seven smaller than the previous experiment of Kimura et al. [10] and Albrow et al. [11]. They cover a momentum range from 497 to 1550 MeV/c in steps of about 100 MeV/c and are therefore a good means to check models of baryon antibaryon scattering.

The differential cross section data are comparable in quality with previous data from Eisenhandler et al. [6] and Kageyama et al. [8]. The shape of the data as expressed in the Legendre coefficients agrees with these previous experiments. The absolute normalization is 10-20% lower than Eisenhandler et al., but is consistent with Kageyama et al.

All potential models considered, are capable of explaining the gross features of the data, but not the details. The central dip in the asymmetry is always too pronounced: the models predict large negative asymmetries that are not seen.

We gratefully acknowledge the assistance of CERN, in particular the LEAR operating crew.

**References**


[1] R.A.Bryan, R.J.N.Phillips, Nucl. Phys. B5 (1968) 201.
[2] C.B.Dover, J.M.Richard, Phys. Rev. C21 (1980) 1466.
C.B.Dover, J.M.Richard, Phys. Rev. C25 (1982) 1952.
[3] J.Côté et al., Phys. Rev. Lett. 48 (1982) 1319.
[4] T.Hippchen et al., preprint without number. Submitted to Phys. Rev. C.
[5] P.H.Timmers et al., Phys. Rev. D29 (1984) 1928.
[6] E.Eisenhandler et al., Nucl. Phys. B113 (1976) 1.
[7] W.Brückner et al., Phys. Lett. 166B (1986) 113.
[8] T.Kageyama et al., Phys. Rev. D35 (1987) 2655.
[9] T.Ohsugi et al., Il Nuovo Cim. A17 (1973) 456.
[10] M.Kimura et al., Proc. of the IV European Symposium on $N\bar{N}$ interactions, 1979, p. 539.
M.Kimura et al., Nuovo Cim. 71A (1982) 438.
[11] M.G.Albrow et al., Nucl. Phys. B37 (1972) 349.
[12] R.A.Kunne, Ph.D. thesis, University of Amsterdam (1988).
[13] E.Aprile et al., in: CERN 81-07, p.124-131.
[14] D.Besset, Ph.D thesis, Université de Genève (1978).
[15] D.Garreta et al., Phys. Lett. 149B (1984) 64.
[16] W.Bauhoff, Atomic data and Nuclear data tables 35 (1986) 429.
[17] H.Aihara et al., Nucl. Phys. A360 (1981) 291.
[18] R.A.Kunne et al., Phys. Lett. 206B (1988) 557.
[19] M.Coupland et al., Phys. Lett. 71B (1977) 460.
[20] R.J.Abrams et al., Phys. Rev. D1 (1970) 70.
[21] H.Iwasaki et al., Nucl. Phys. A433 (1985) 433.
[22] K.Nakamura et al., Phys. Rev. D29 (1984) 349.
[23] A.S.Clough et al., Phys. Lett. 146B (1984) 299;
D.V.Bugg et al. Phys. Lett. 194B (1987) 563.
[24] R.P.Hamilton et al., Phys. Rev. Lett 44 (1980) 1182.
[25] M.Cresti et al., Phys. Lett 132B (1983) 209.
[26] W.Brückner et al., Phys. Lett 158B (1983) 180.
[27] P.Jenni et al., Phys. Lett 94B (1981) 1.
[28] The T resonance structure has been seen in:
$\bar{p}p$ and $\bar{p}d$ total elastic cross section, R.J.Abrams et al., Phys. Rev D1 (1970) 1917.
charge exchange cross section, D.Cutts et al., Stony Brook-Wisconsin preprint (1973)
$\bar{p}p \rightarrow \pi^+\pi^-$, A.A.Carter et al., Phys. Lett 67B (1977) 117.
Backward production in $\pi^-p$ interactions, P.Benkheiri et al., Phys. Lett 68B (1977) 483.

**Tables**

| Correction: | Value: |
|---|---|
| Background subtracted | |
| PP: | 12-18% |
| PM: | 15-21% |
| Inefficiency due to chambers: | 20-40% |
| Absorption of secondaries: | 10-15% |
| Geometrical inefficiency: | 0% (see text) |
| Random triggers: | 1-3% |
| Random vetoes: | 0-1% |
| Bad beam: | 1-3% |
| Attenuation of beam | |
| between S3 and target: | 0.5-0.8% |
| inside target: | 3-7% |
| Effective target length: | 0.2-0.6% |

*Table 1: Values of the applied corrections.*

| Systematic error source: | Error: |
|---|---|
| Position S3 | +6% |
| Density of target | ±8% |
| Absorption of secondaries: | ±2% |
| Straggling: | +2% |
| Inefficiency calculation: | ±2% |
| Shape of background: | ±2% |
| Target polarization: | ±4% |
| Added in quadrature: | +11.3% −9.6% |
| Idem asymmetry: | ±4.5% |

*Table 2: Dominant systematic errors.*

| Momentum range (MeV/c) | Normalization | Reference with year |
|---|---|---|
| 487-737 | 0.98 | Nakamura et al., 1984 [22] |
| 484-599 | 1.03 | Clough et al., 1984 [23] |
| 480-1066 | 0.99 | Hamilton et al., 1980 [24] |
| 1000-1600 | 1.01 | Abrams et al., 1970 [20] |

*Table 3: Total cross section data samples*

| Momentum range (MeV/c) | Reference with year |
|---|---|
| 479-578 | Cresti et al., 1983 [25] |
| 505,590 | Brückner et al., 1983 [26] |
| 1174-2607 | Jenni et al., 1981 [27] |
| 481-715 | Iwasaki et al., 1985 [21] |

*Table 4: ρ data sample*

| | This experiment Fit to $A_{on}$ and $d\sigma/d\Omega$ data together | Fit to $d\sigma/d\Omega$ data only | Eisenhandler et al. Fit to $d\sigma/d\Omega$ using our procedure for normalization | Data of ref. [9] |
|---|---|---|---|---|
| $a_0$ | 2.89±.07 | 2.99±.08 | 3.41±.12 | 3.39±.05 |
| $a_1/a_0$ | 2.82±.09 | 2.76±.09 | 2.50±.06 | 2.53±.06 |
| $a_2/a_0$ | 3.41±.14 | 3.38±.14 | 3.34±.14 | 3.19±.07 |
| $a_3/a_0$ | 3.81±.18 | 3.66±.17 | 3.15±.13 | 2.99±.08 |
| $a_4/a_0$ | 2.73±.15 | 2.66±.15 | 2.57±.14 | 2.15±.07 |
| $a_5/a_0$ | 2.21±.12 | 2.05±.11 | 1.49±.09 | 1.17±.06 |
| $a_6/a_0$ | 1.04±.06 | 1.00±.06 | 0.85±.05 | 0.48±.03 |
| $a_7/a_0$ | 0.78±.03 | 0.70±.03 | 0.32±.02 | 0.17±.01 |
| $a_8/a_0$ | 0.22±.01 | 0.21±.01 | 0.16±.01 | 0.04±.01 |
| $\chi^2$/DF | 1.8 | 3.3 | 1.0 | 1.0 |

*Table 5: Comparison of different fits at 1089 MeV/c.*

| p (MeV/c) | $\sigma_{tot}$ (mb) | $\rho$ | $\frac{d\sigma(0^0)}{d\Omega}$ (mb/sr) | b ($GeV^{-2}/c^{-2}$) | $\sigma_{el}$ (mb) |
|---|---|---|---|---|---|
| 679 | 141.5 | 0.25 | 35.7 | 18.6 | 44.5±3.1 |
| 783 | 131.3 | 0.29 | 40.6 | 16.6 | 43.2±3.0 |
| 886 | 123.6 | 0.31 | 45.1 | 15.5 | 41.6±2.9 |
| 988 | 117.5 | 0.31 | 49.0 | 15.1 | 41.2±2.9 |
| 1089 | 112.6 | 0.30 | 52.6 | 15.0 | 36.3±2.5 |
| 1190 | 108.5 | 0.28 | 55.9 | 15.1 | 36.6±2.6 |
| 1291 | 105.0 | 0.26 | 59.0 | 15.3 | 36.4±2.5 |
| 1400 | 101.9 | 0.23 | 62.2 | 15.3 | 34.3±2.4 |
| 1416 | 101.4 | 0.22 | 62.7 | 15.2 | 34.6±2.4 |
| 1449 | 100.6 | 0.21 | 63.7 | 15.1 | 35.8±2.5 |
| 1467 | 100.2 | 0.21 | 64.2 | 15.1 | 33.0±2.3 |
| 1501 | 99.4 | 0.20 | 65.2 | 14.9 | 31.0±2.2 |
| 1550 | 98.2 | 0.19 | 66.6 | 14.5 | 30.0±2.1 |

*Table 6: The total elastic cross section*

**Figure captions**

Figure 1: Schematic view of the experimental setup. B0,S1,S2,S3: beam defining counters; B,J,C,L,R: multiple wire proportional chambers; HL,HR: hodoscope counters; M: polarized target magnet; P: cryostat with polarized target; beam: incident and throughgoing beam track;

Figure 2: $\chi^2$ distribution for 1089 MeV/c after selections (PP and PM combined). Shaded histogram: background calculated from the dummy target measurement.

Figure 3: Efficiencies for 1089 MeV/c. Upper plots: Target polarization 'up'. Lower plots: Target polarization 'down'. Left side plots: PP events. Right side plots: PM events.

Figure 4: $A_{on}$ 497 and 523 MeV/c.

Figure 5: $A_{on}$ and $d\sigma/d\Omega$ for 679, and 783 MeV/c. The curves are the Legendre fits to the data described in the text.

Figure 6: $A_{on}$ and $d\sigma/d\Omega$ for 886 and 988 MeV/c. The curves are the Legendre fits to the data described in the text.

Figure 7: $A_{on}$ and $d\sigma/d\Omega$ for 1089 and 1190 MeV/c. The curves are the Legendre fits to the data described in the text.

Figure 8: $A_{on}$ and $d\sigma/d\Omega$ for 1291 and 1400 MeV/c. The curves are the Legendre fits to the data described in the text.

Figure 9: $A_{on}$ and $d\sigma/d\Omega$ for 1416 and 1449 MeV/c. The curves are the Legendre fits to the data described in the text.

Figure 10: $A_{on}$ and $d\sigma/d\Omega$ for 1467 and 1501 MeV/c. The curves are the Legendre fits to the data described in the text.

Figure 11: $A_{on}$ and $d\sigma/d\Omega$ for 1550 MeV/c. The curves are the Legendre fits to the data described in the text.

Figure 12: Differential cross sections at 783 MeV/c and 1089 MeV/c. The curves are the Legendre fits to the data of Kageyama et al. [8] at 790 MeV/c (labeled K) and Eisenhandler et al. [6] at 780 and 1090 MeV/c (labeled E).

Figure 13: The forward nuclear differential cross section. Present calculation (solid line with error bars) compared with the result of Coupland et al. (dashed line) [19].

Figure 14: The normalization parameter

Figure 15: Legendre coefficients $a_1$ up to $a_4$ normalized by $a_0$ (closed squares). The results are compared with ref. [8] (closed circles) and [6] (open diamonds). For all points shown the diagonal errors are typical 0.1.

Figure 16: Legendre coefficients $a_5$ up to $a_8$ normalized by $a_0$ (closed squares). The results for $a_5$ are compared with ref. [8] (closed circles) and [6] (open diamonds). For all points shown the diagonal errors are typical 0.1.

Figure 17: Legendre coefficients $b_1$ up to $b_4$ normalized by $a_0$ (closed squares). For all points shown the diagonal errors are typical 0.01.

Figure 18: Legendre coefficients $b_5$ up to $b_8$ normalized by $a_0$ (closed squares). For all points shown the diagonal errors are typical 0.005.

Figure 19: The total elastic cross section.

Figure 20: Comparison of the asymmetry data (closed squares) with the data from previous experiments (open circles). Left: $A_{on}$ at 679 MeV/c (this exp.) and at 699 MeV/c (Kimura et al.). Right: $A_{on}$ at 886 MeV/c (this exp.) and at 910 MeV/c (Albrow et al.).

Figure 21: Model predictions for the asymmetry at 679 MeV/c. The data points are those of this experiment. The curves are the prediction of the Paris model (full curve), Dover-Richard model II (dashed curve), Nymegen potential (dotted curve) and Bonn potential (crossed-dashed curve).

Figure 22: Position of the extrema in the differential cross section and asymmetry data compared with the predictions of the Paris model. The curves are: prediction for the position of the diffraction minimum (solid line), $A_{max}$ (dashed-crossed line) and $A_{min}$ (dashed line).

Figure 23: Value of the central minimum in the asymmetry data compared with the predictions of the Paris model.

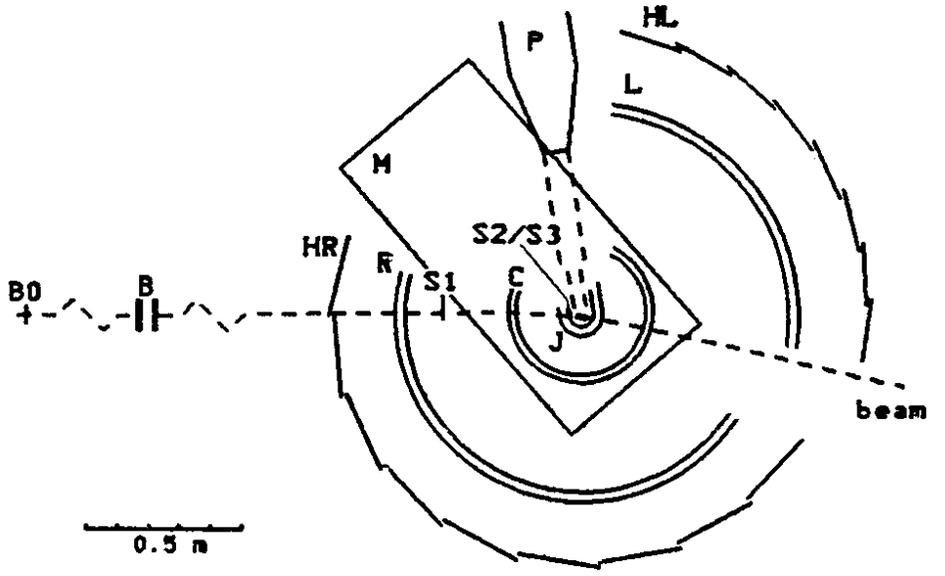


*Figure 1: Schematic view of the experimental setup.*

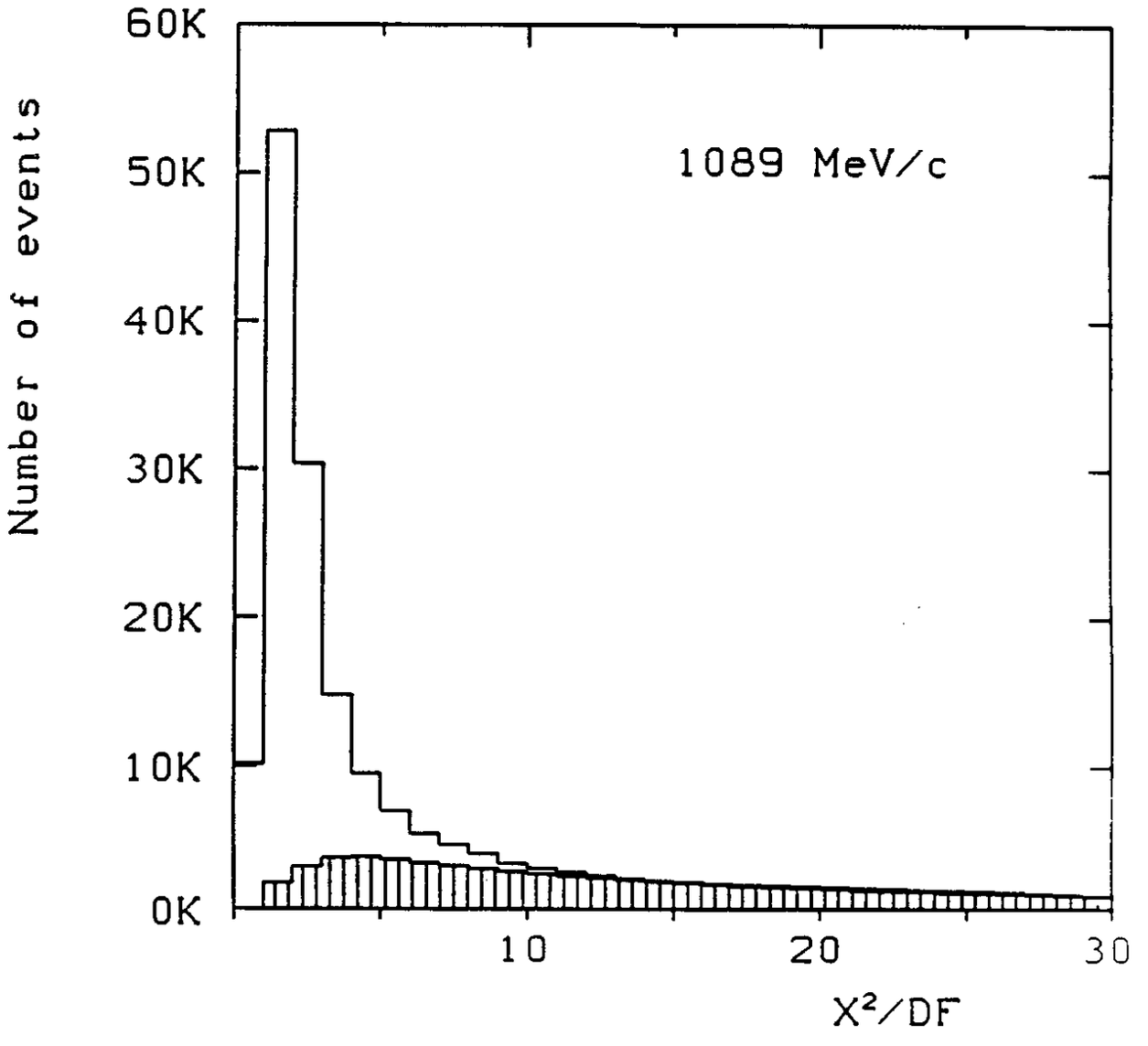


*Figure 2: $\chi^2$ distribution for 1089 MeV/c*

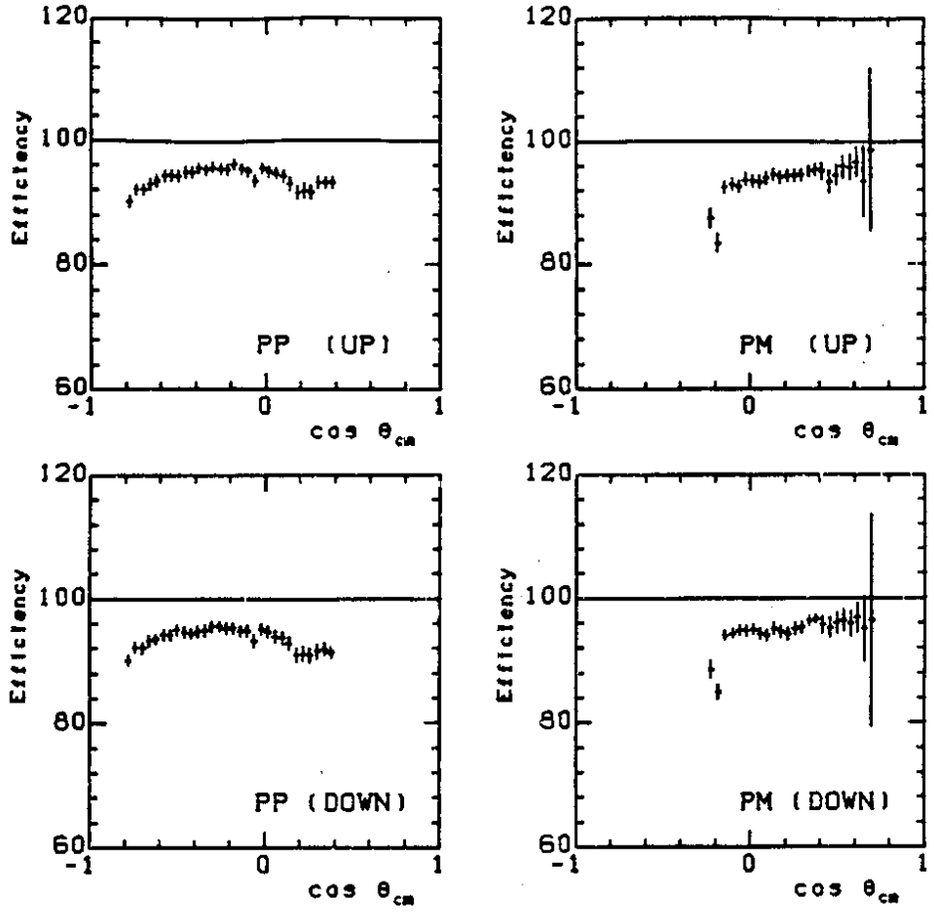


*Figure 3:. Efficiencies for 1089 MeV/c.*

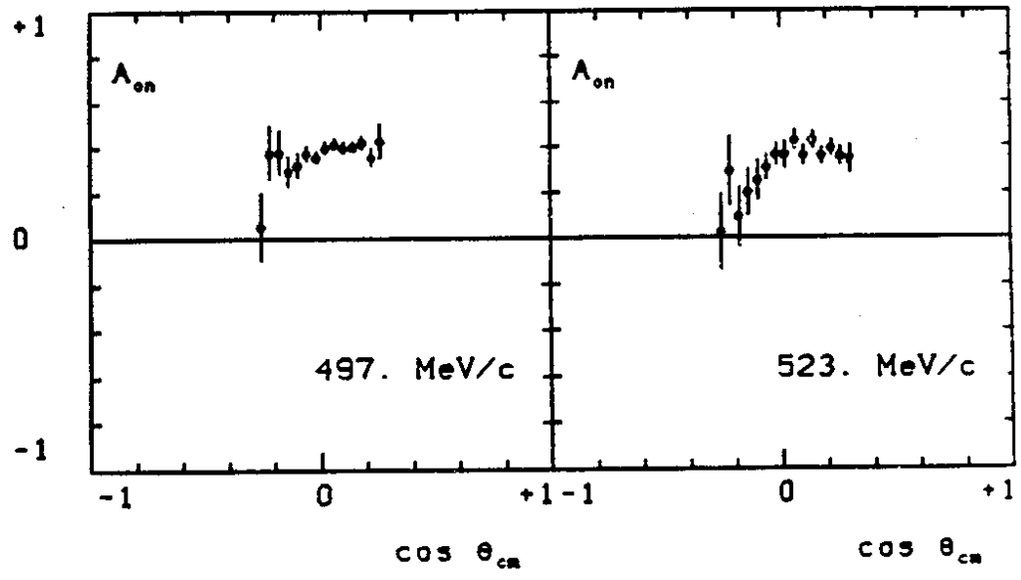


*Figure 4: $A_{on}$ 497 and 523 MeV/c.*

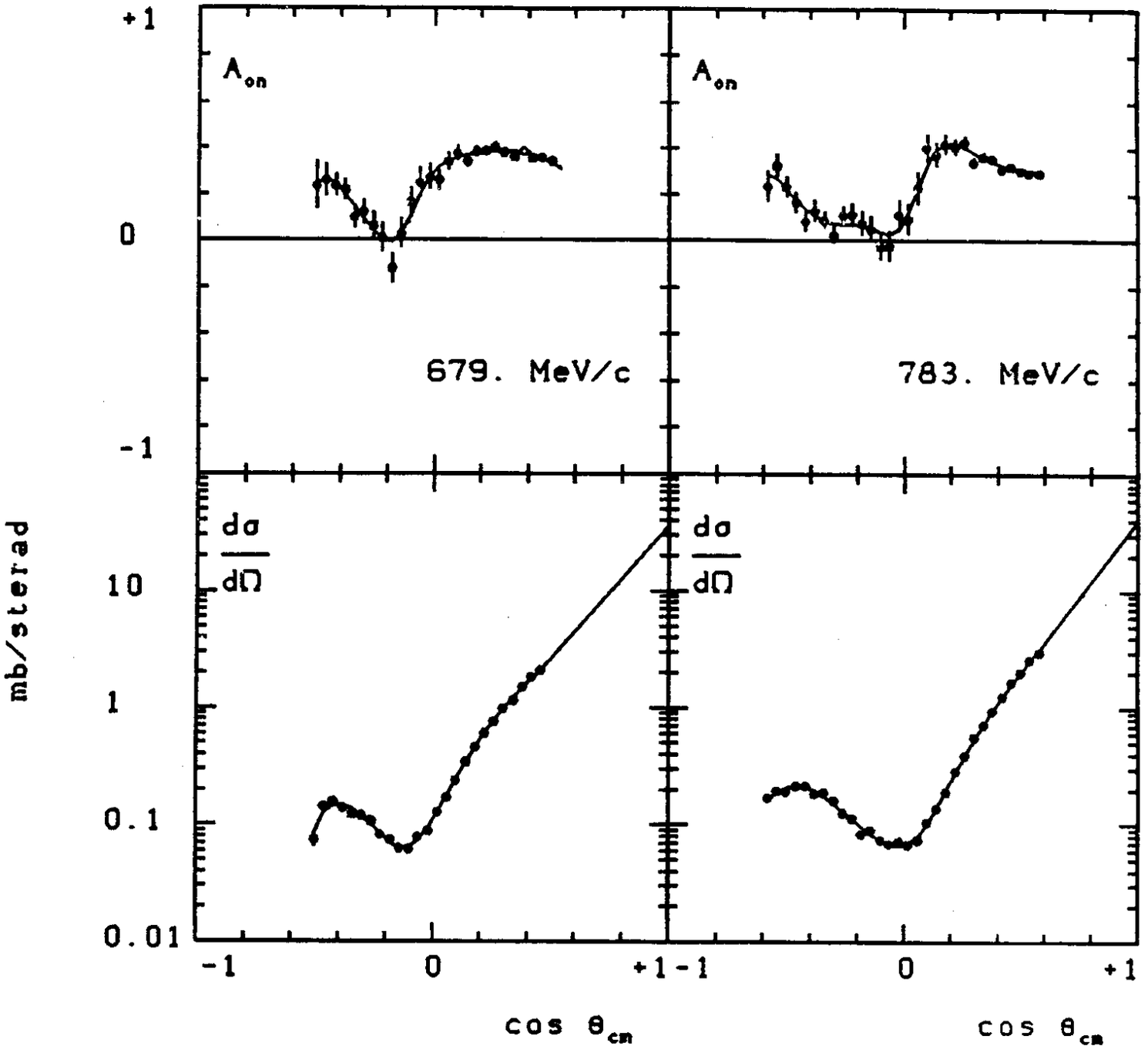
+1
0
-1
$A_{on}$
679. MeV/c
783. MeV/c
$\frac{d\sigma}{d\Omega}$
mb/sterad
10
1
0.1
0.01
-1
0
+1
cos $\theta_{cm}$

*Figure 5*

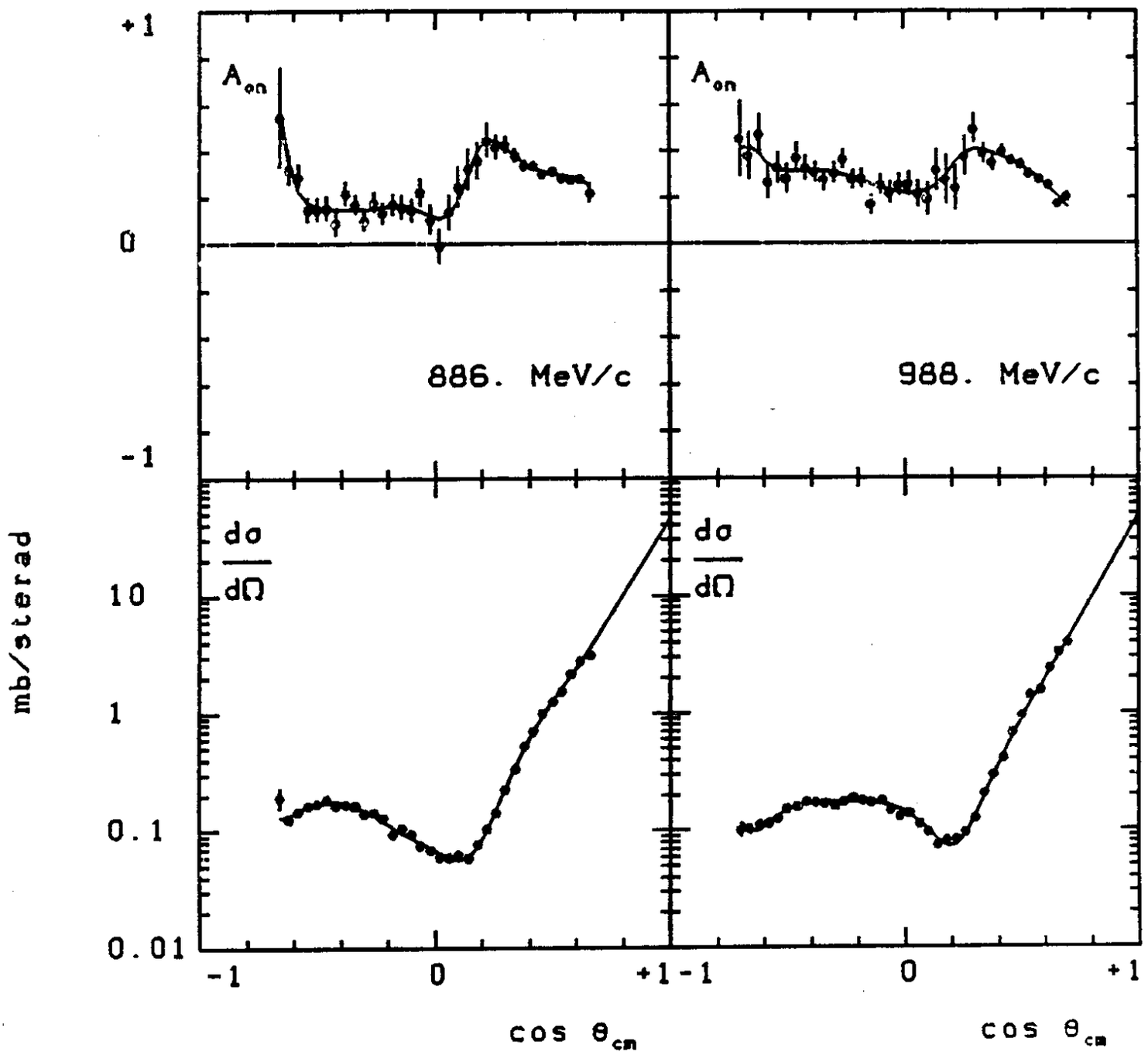
+1
0
-1
$A_{on}$
886. MeV/c
988. MeV/c
$\frac{d\sigma}{d\Omega}$
mb/sterad
10
1
0.1
0.01
-1
0
+1
cos $\theta_{cm}$

*Figure 6*

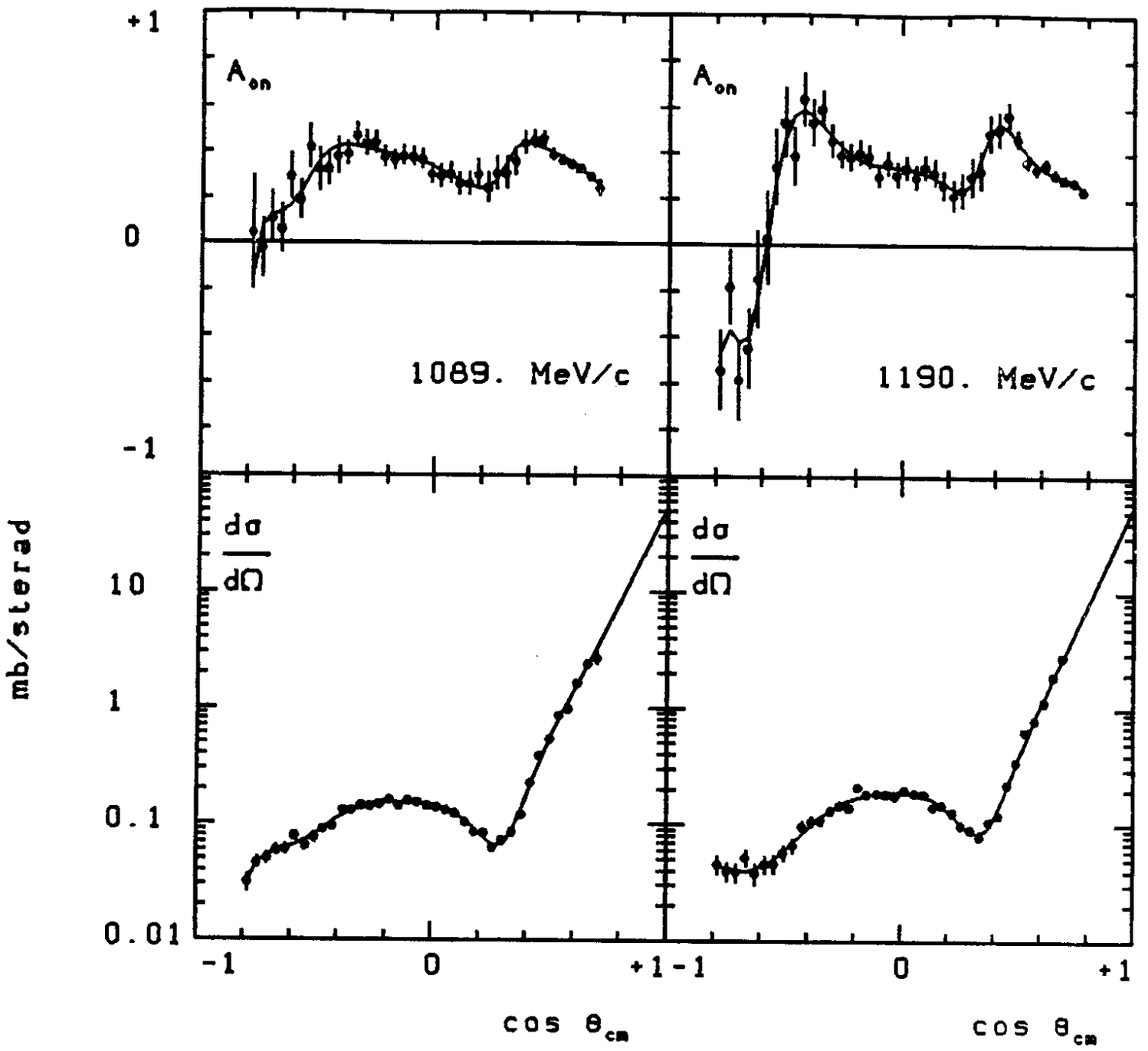
+1
0
-1
$A_{on}$
1089. MeV/c
1190. MeV/c
mb/sterad
10
1
0.1
0.01
$\frac{d\sigma}{d\Omega}$
-1
0
+1
cos $\theta_{cm}$

*Figure 7*

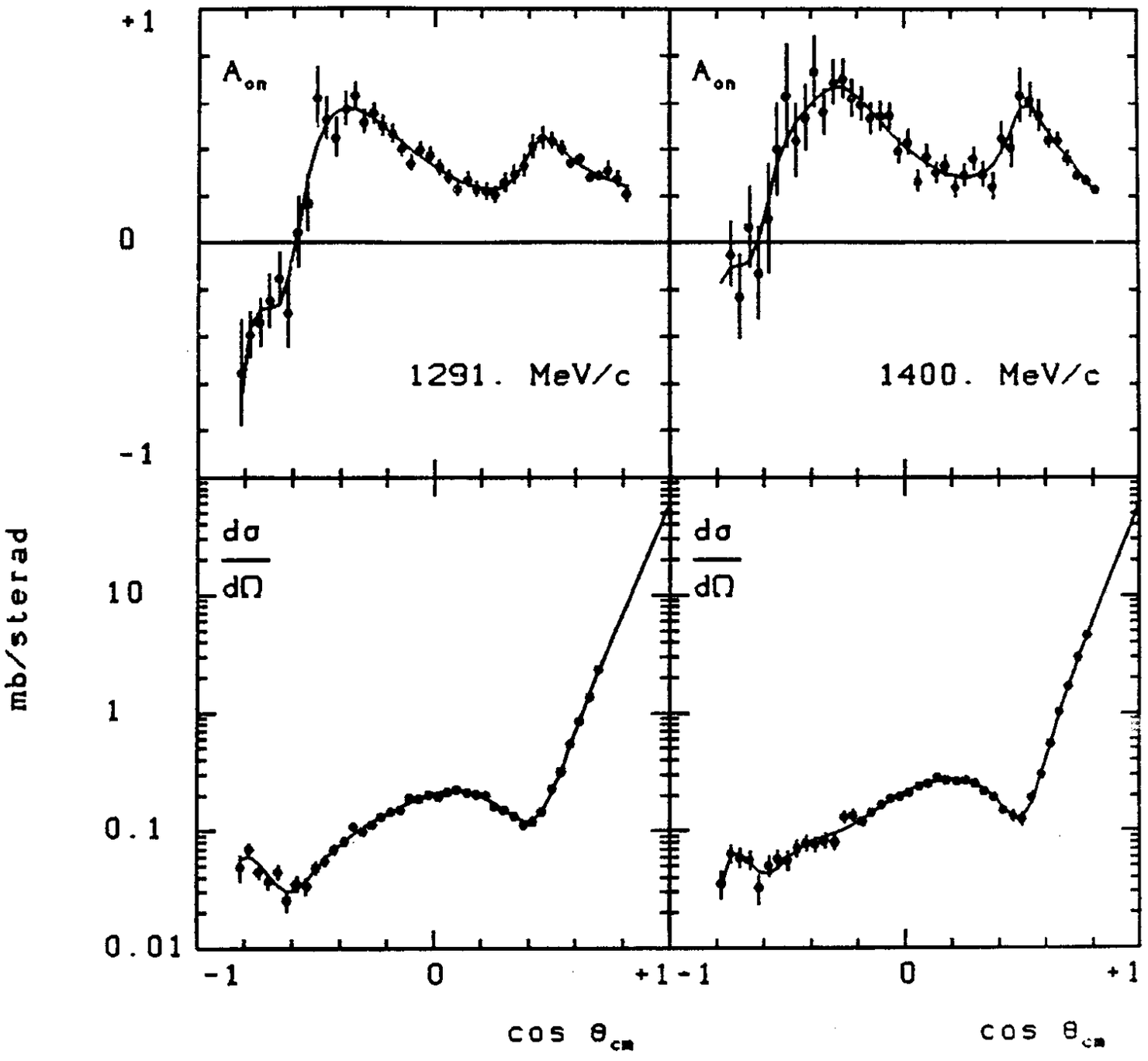
+1
0
-1
$A_{on}$
1291. MeV/c
1400. MeV/c
$\frac{d\sigma}{d\Omega}$
mb/sterad
10
1
0.1
0.01
-1
0
+1
cos $\theta_{cm}$

*Figure 8*

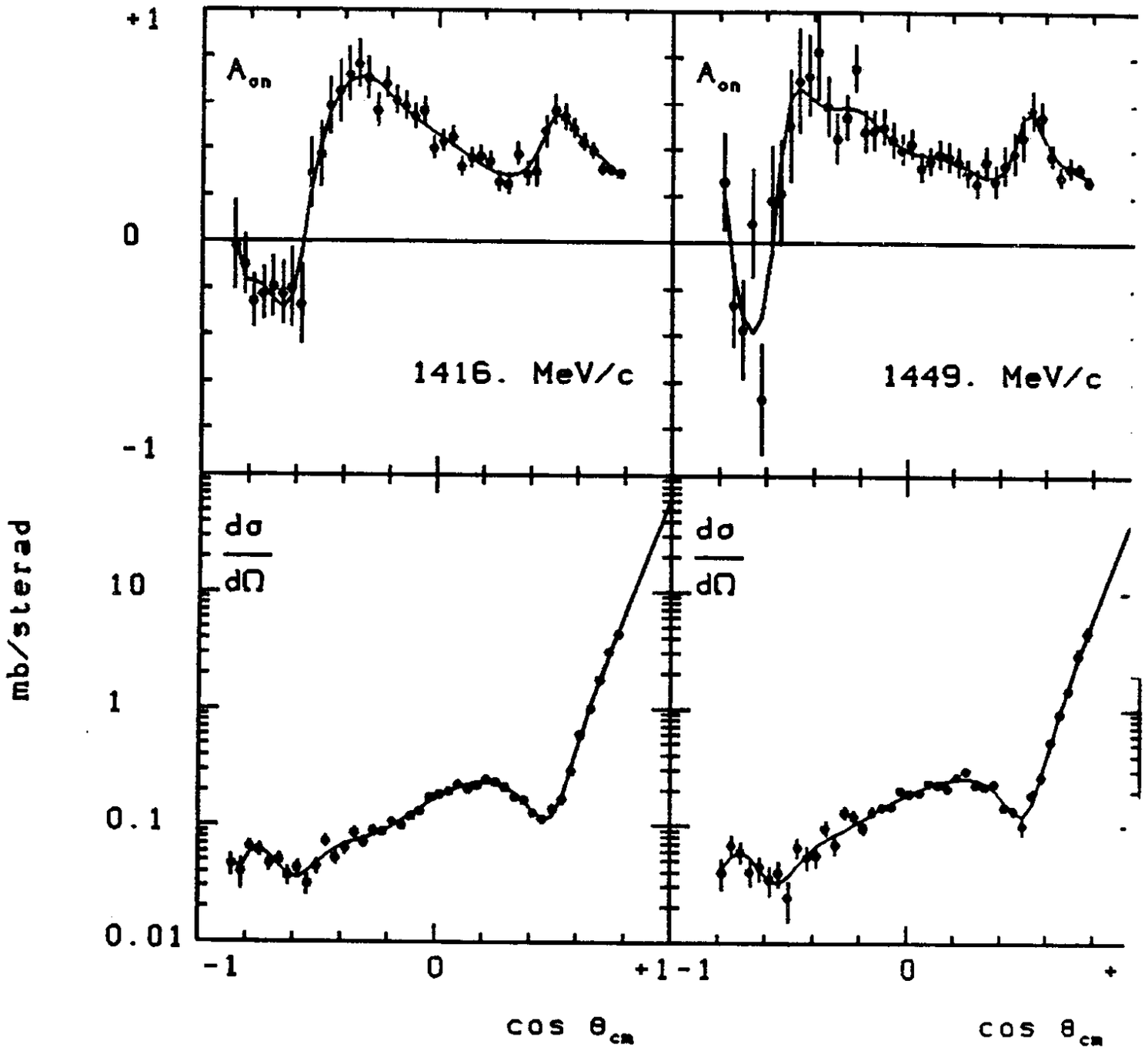
+1
0
-1
$A_{on}$
1416. MeV/c
1449. MeV/c
$\frac{d\sigma}{d\Omega}$
10
1
0.1
0.01
mb/sterad
-1
0
+1
cos $\theta_{cm}$

*Figure 9*

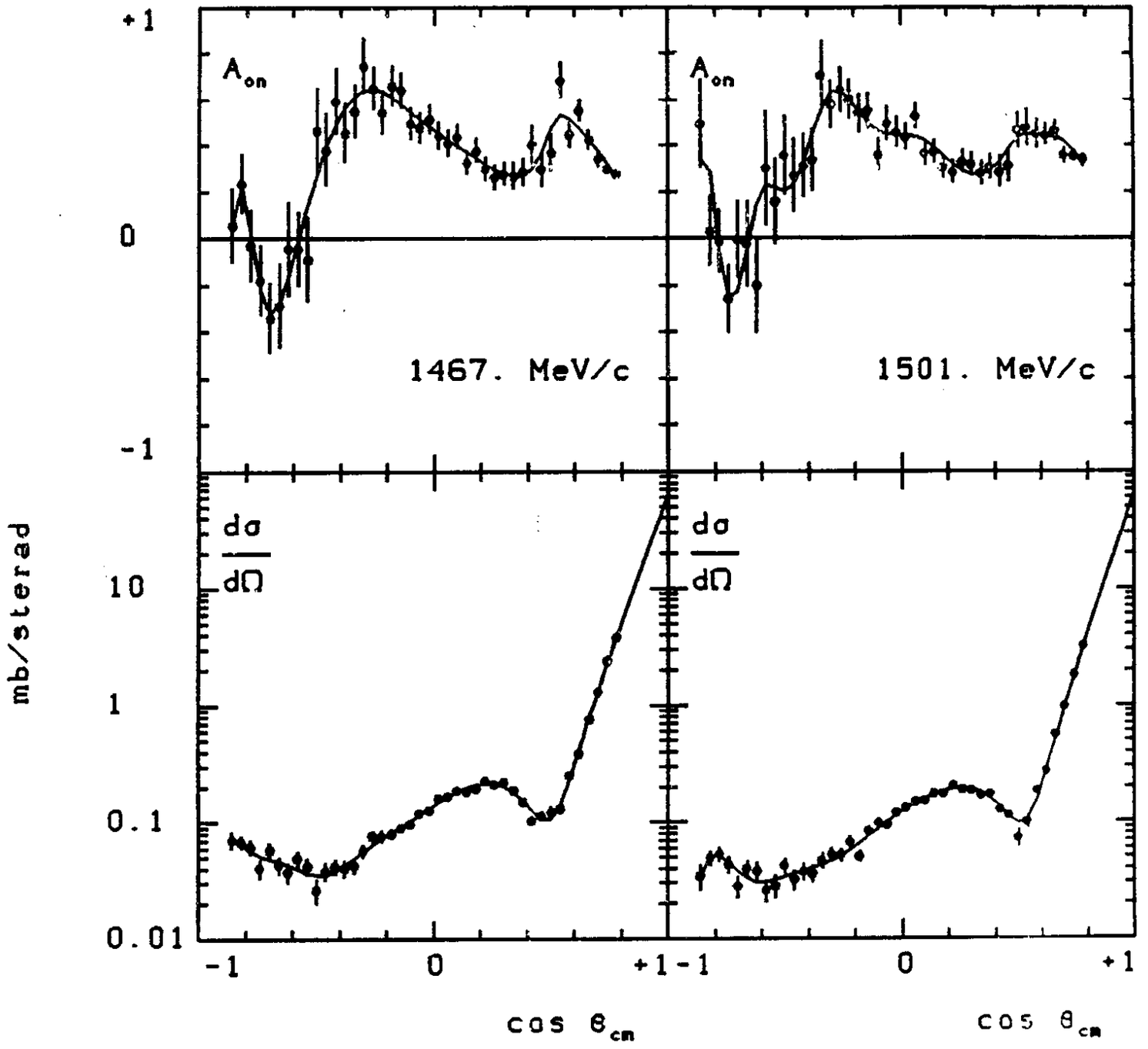
+1
0
-1
$A_{on}$
1467. MeV/c
1501. MeV/c
$\frac{d\sigma}{d\Omega}$
10
1
0.1
0.01
mb/sterad
-1
0
+1
cos $\theta_{cm}$

*Figure 10*

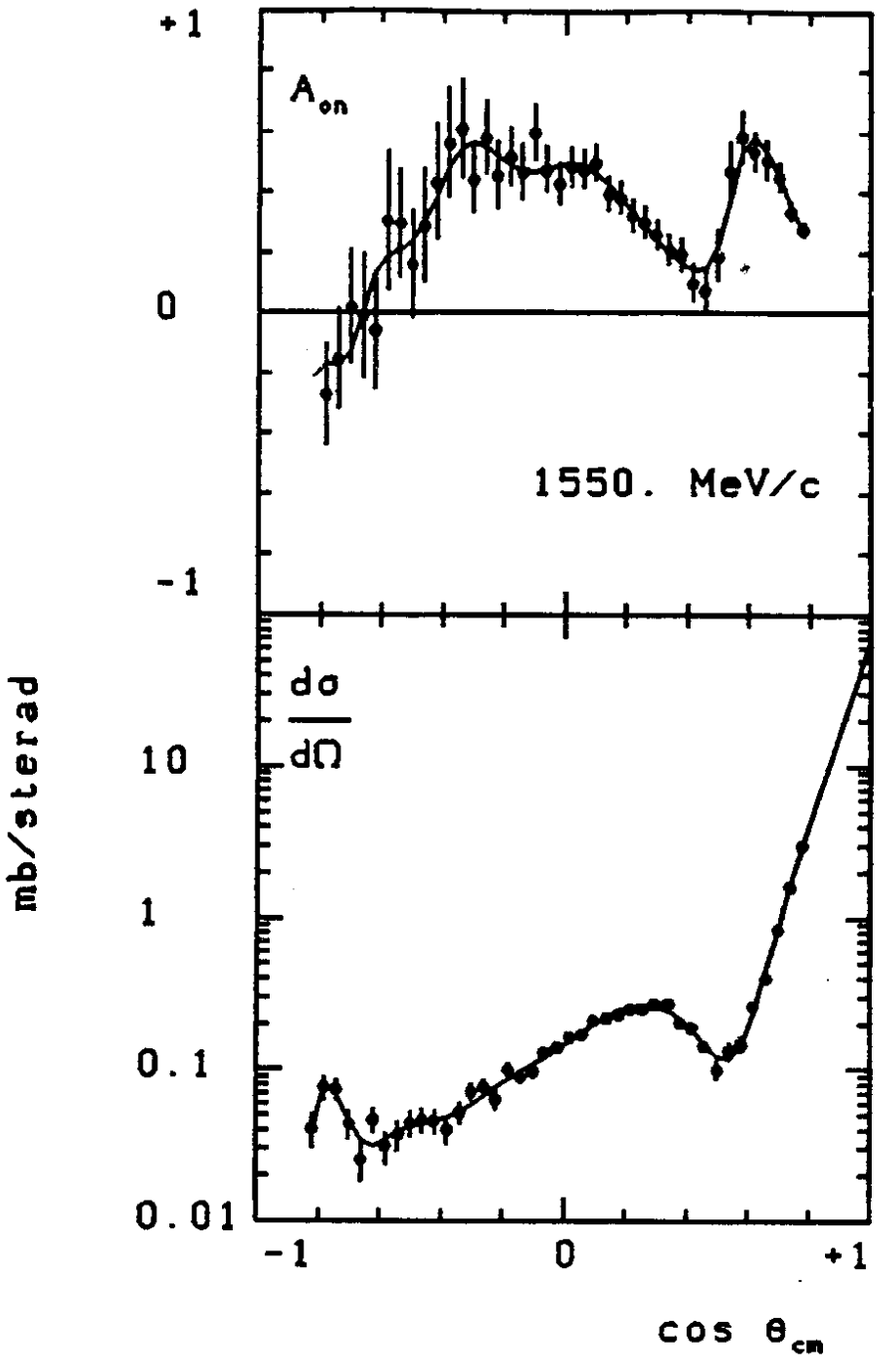
+1
$A_{on}$
0
1550. MeV/c
-1
$\frac{d\sigma}{d\Omega}$
mb/sterad
10
1
0.1
0.01
-1
0
+1
cos $\theta_{cm}$

*Figure 11*

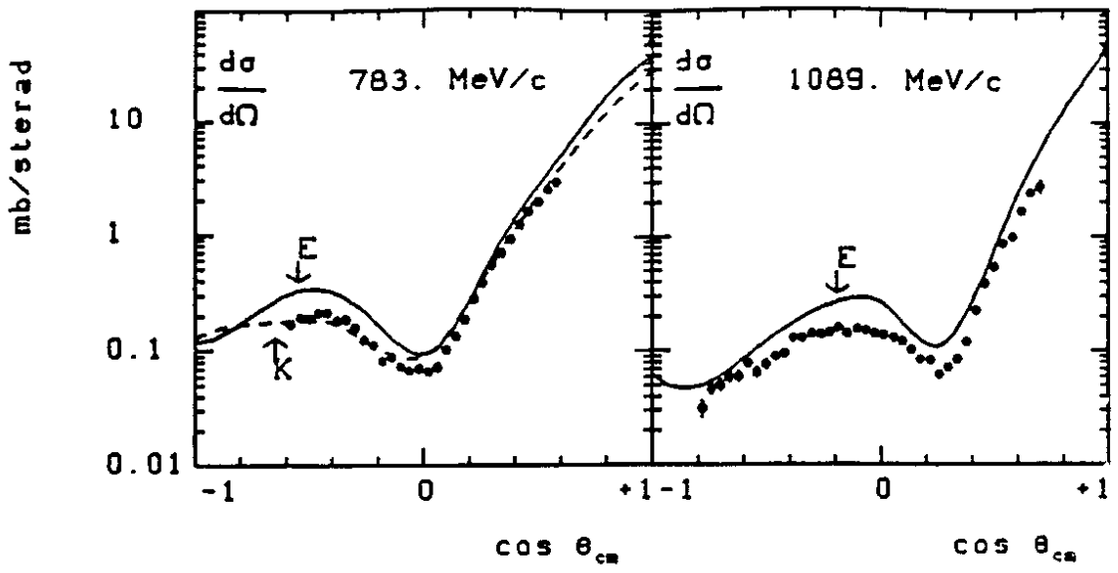


*Figure 12: Differential cross sections at 783 MeV/c and 1089 MeV/c.*

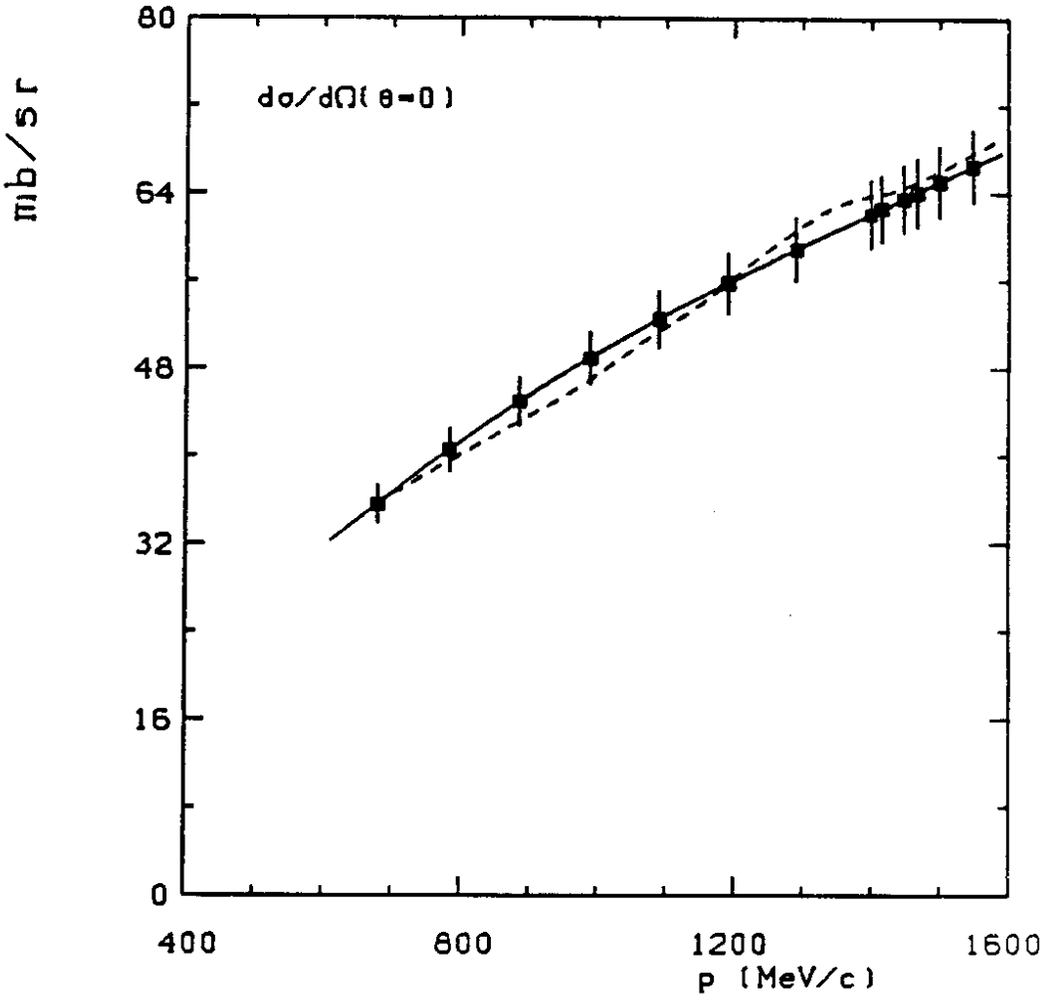


*Figure 13: The forward nuclear differential cross section.*

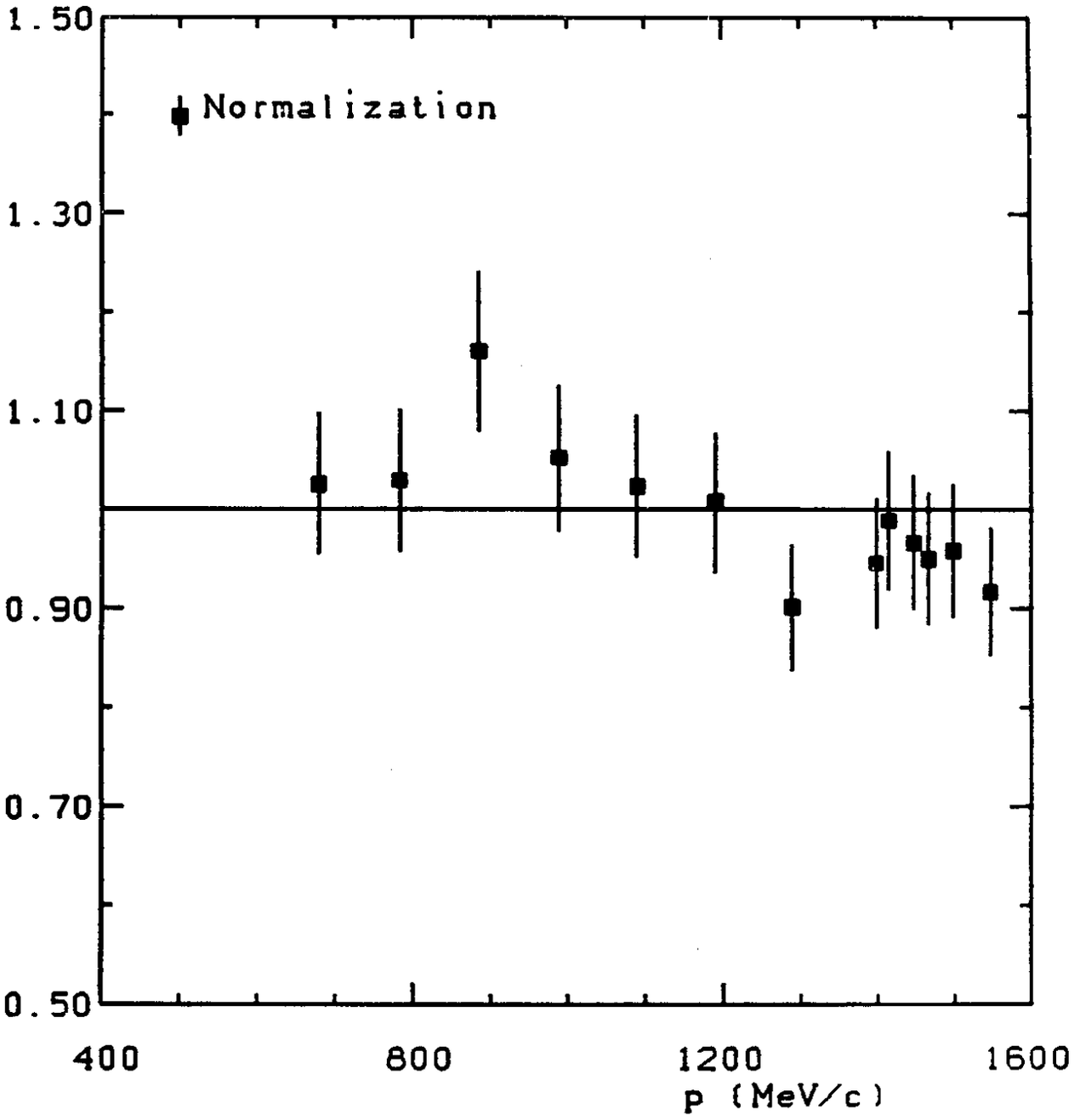
1.50
1.30
1.10
0.90
0.70
0.50
Normalization
400
800
1200
1600
p (MeV/c)

*Figure 14*

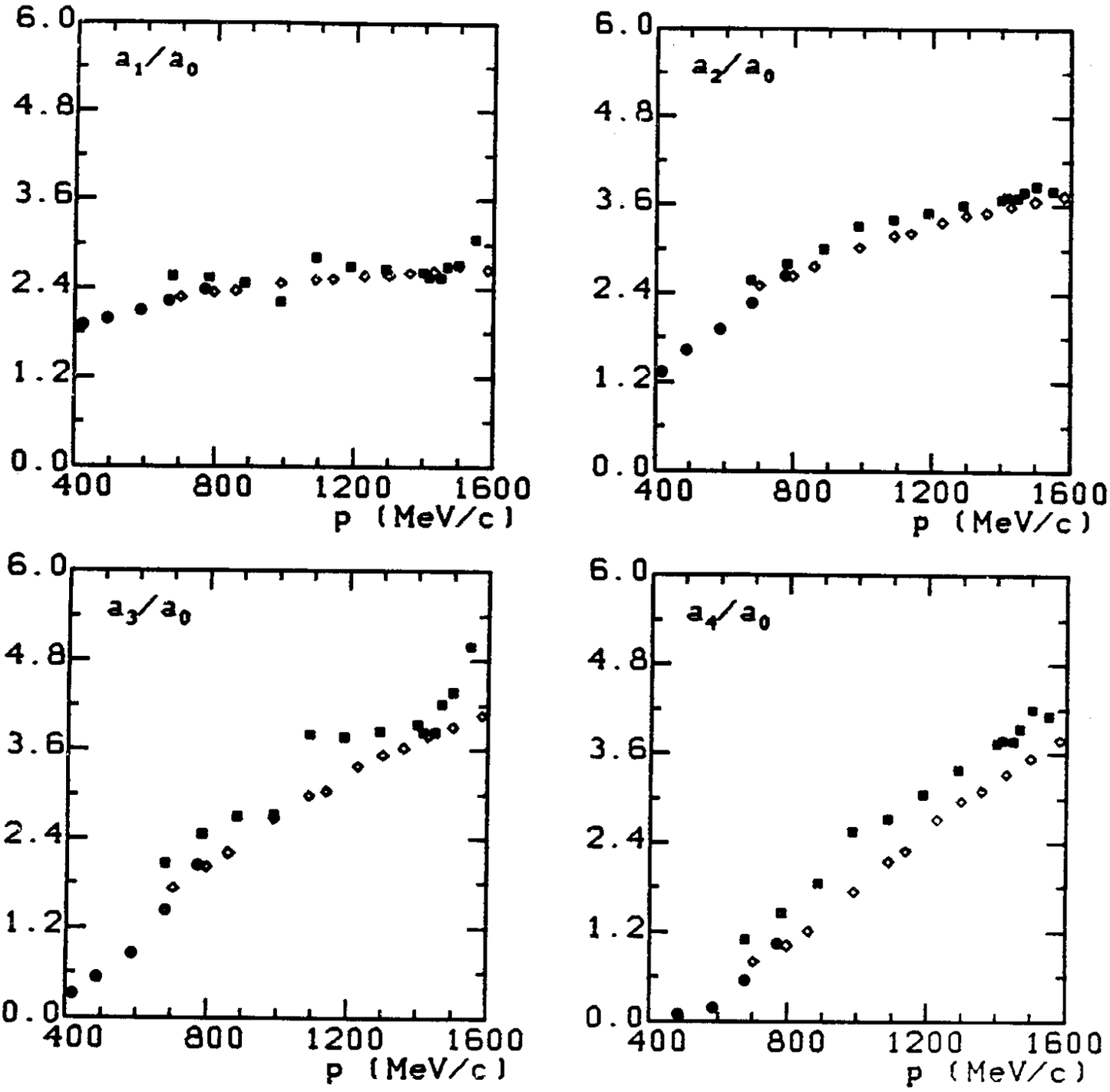


*Figure 15: Legendre coefficients*

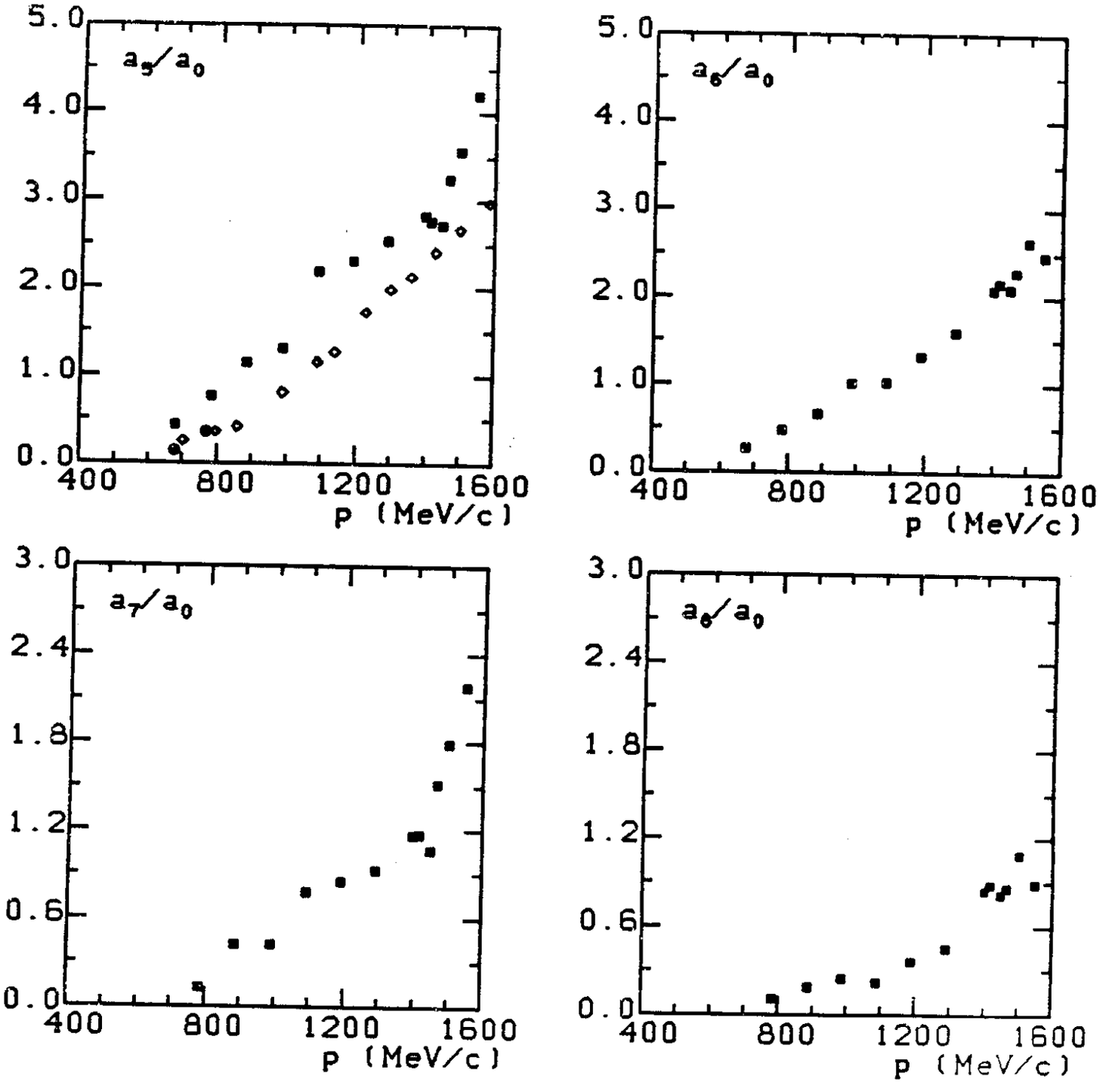


*Figure 16: Legendre coefficients*

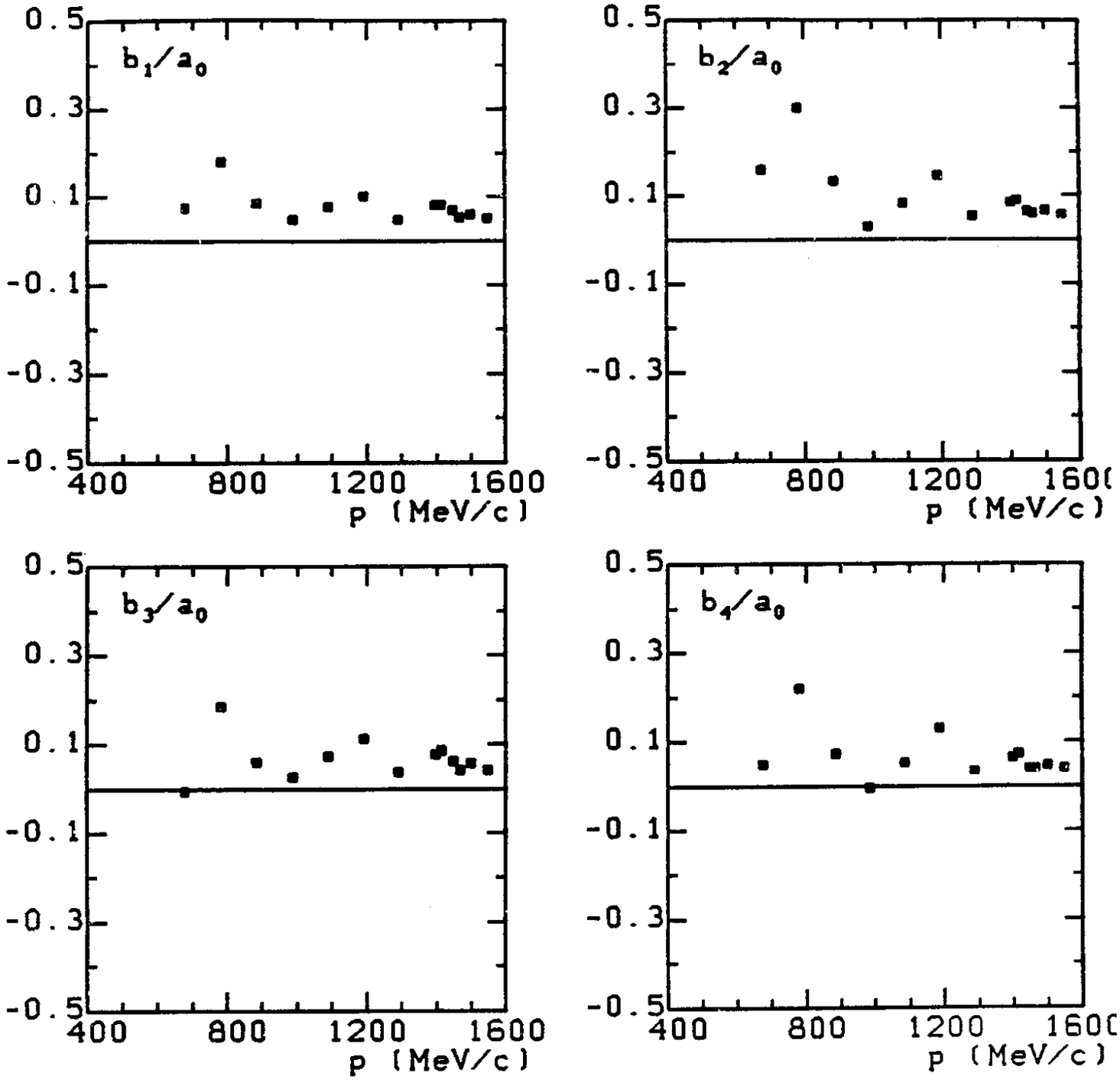


*Figure 17: Legendre coefficients*

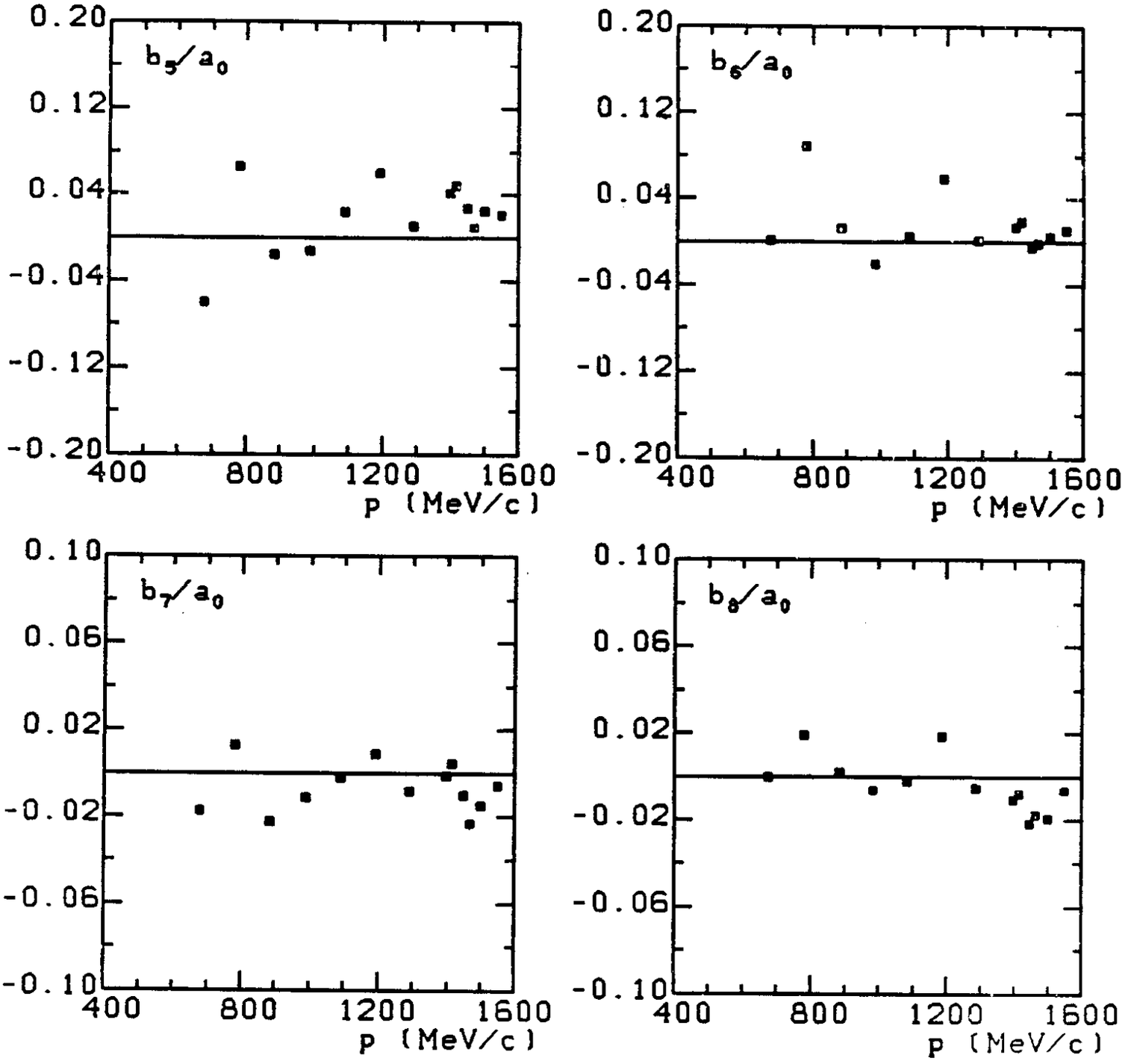


*Figure 18: Legendre coefficients*

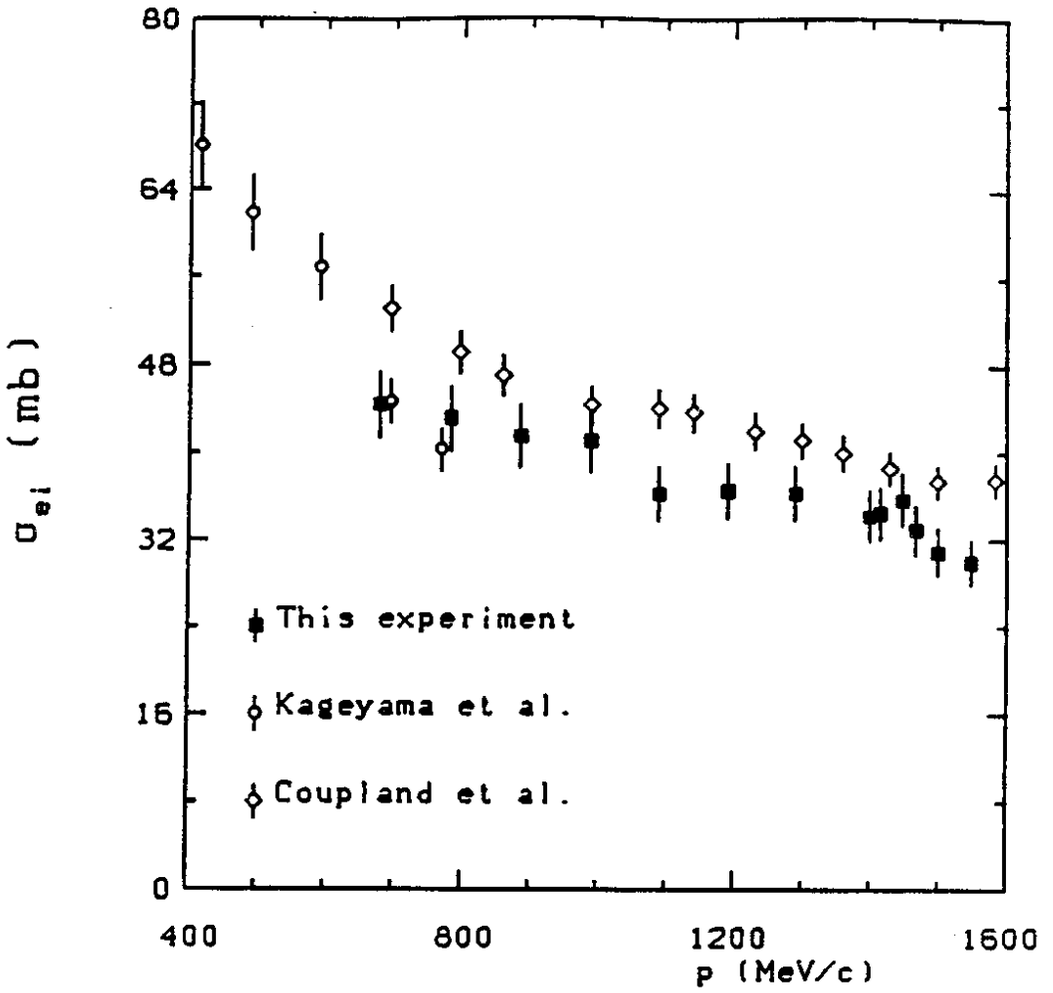


*Figure 19: The total elastic cross section.*

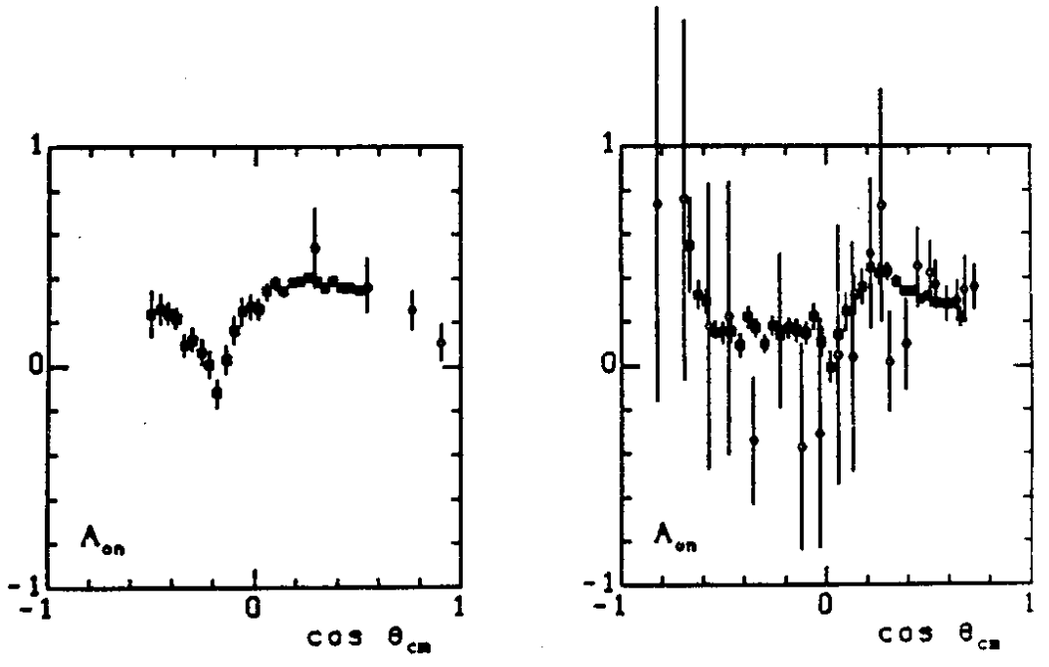


*Figure 20: Comparison of the asymmetry data*

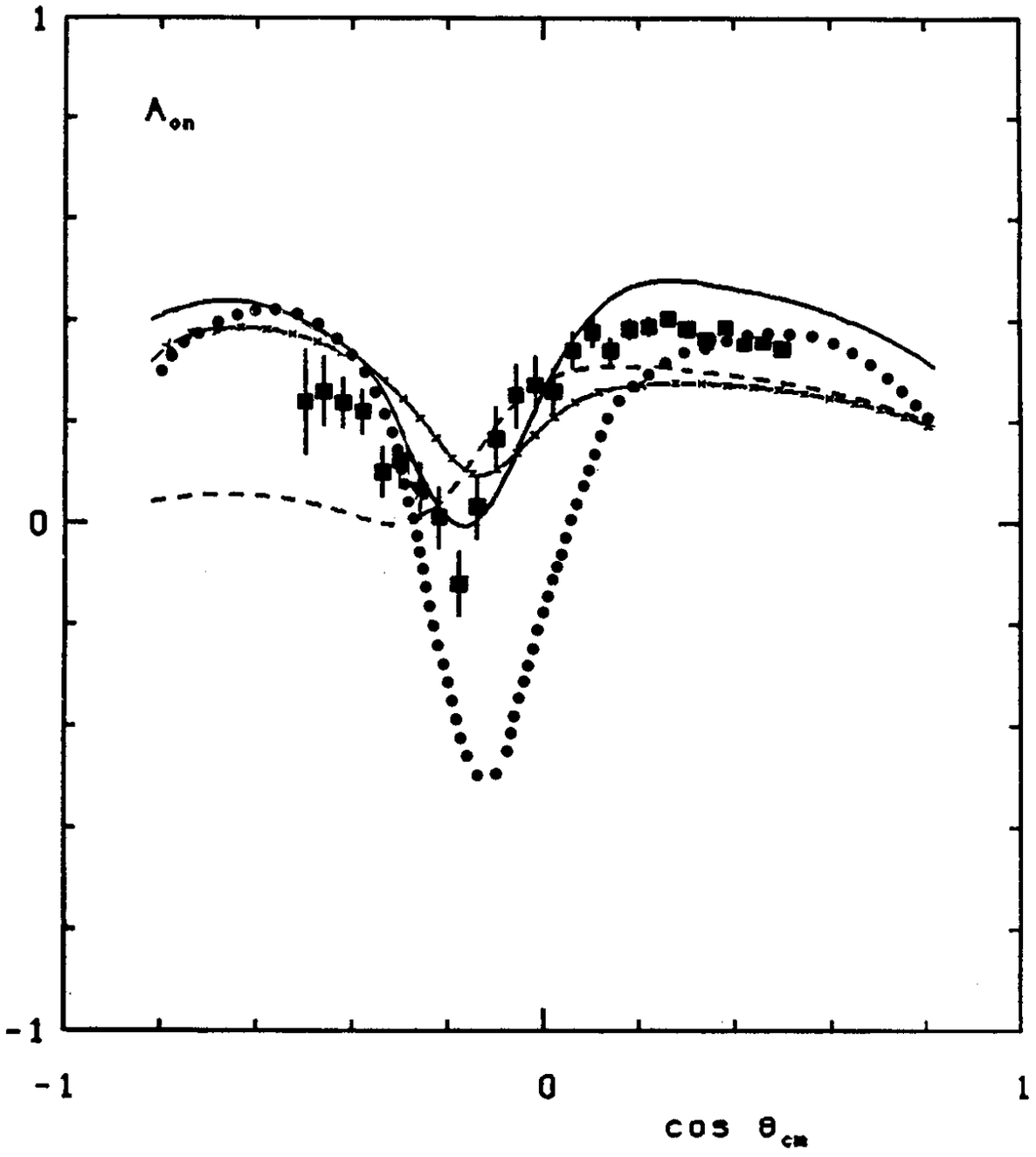


*Figure 21: Model predictions for the asymmetry at 679 MeV/c.*

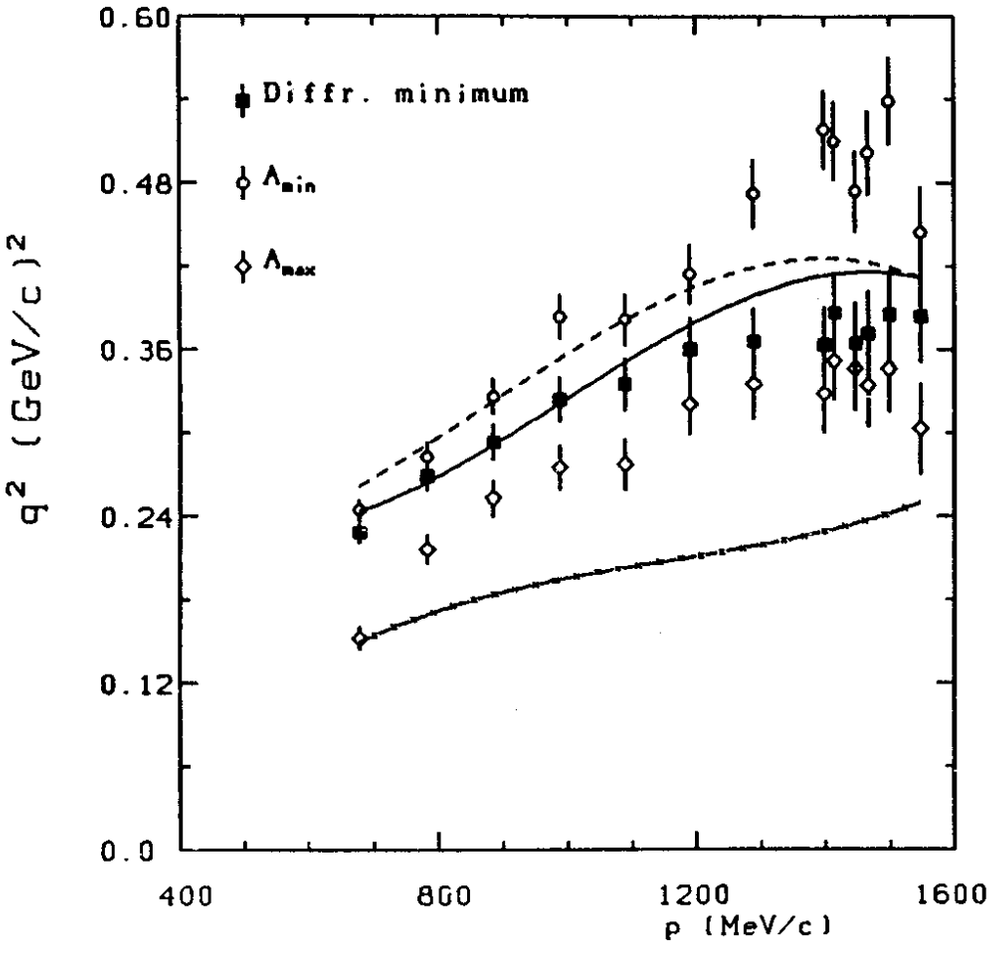


*Figure 22*

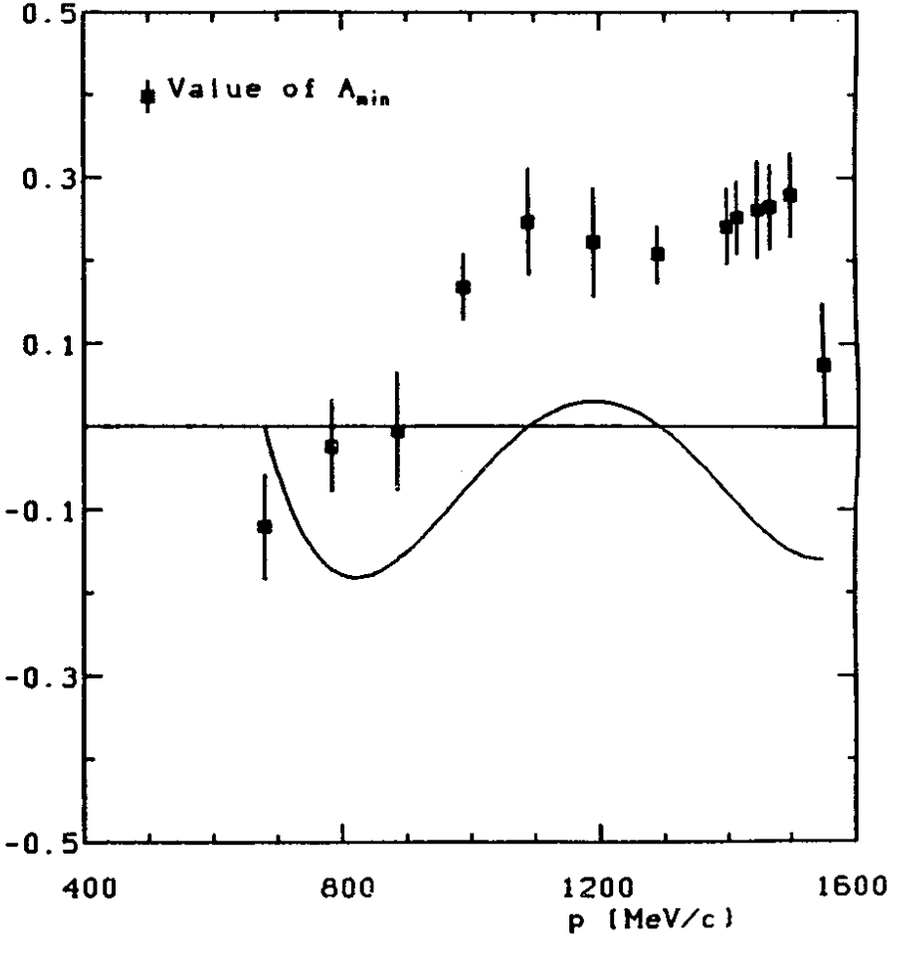


*Figure 23*

## APPENDIX A

Numerical values for $A_{on}$ and $d\sigma/d\Omega$

The differential cross sections given are normalized according to the procedure described in Chapter 4.

| cosθ | A | cosθ | A |
|---|---|---|---|
| -0.26 | 0.05±0.15 | 0.02 | 0.40±0.03 |
| -0.22 | 0.38±0.12 | 0.06 | 0.42±0.03 |
| -0.18 | 0.38±0.10 | 0.10 | 0.40±0.02 |
| -0.14 | 0.30±0.07 | 0.14 | 0.41±0.02 |
| -0.10 | 0.33±0.05 | 0.18 | 0.43±0.03 |
| -0.06 | 0.38±0.03 | 0.22 | 0.36±0.04 |
| -0.02 | 0.36±0.03 | 0.26 | 0.43±0.08 |

Table 1: Momentum in centre of target: 497 MeV/c

| cosθ | A | cosθ | A |
|---|---|---|---|
| -0.26 | 0.03±0.17 | 0.06 | 0.43±0.04 |
| -0.22 | 0.29±0.15 | 0.10 | 0.36±0.04 |
| -0.18 | 0.09±0.13 | 0.14 | 0.43±0.04 |
| -0.14 | 0.20±0.10 | 0.18 | 0.36±0.03 |
| -0.10 | 0.25±0.09 | 0.22 | 0.39±0.03 |
| -0.06 | 0.31±0.06 | 0.26 | 0.36±0.04 |
| -0.02 | 0.36±0.05 | 0.30 | 0.35±0.06 |
| 0.02 | 0.37±0.06 | | |

Table 2: Momentum in centre of target: 523 MeV/c

| cosθ | A | dσ/dΩ | cosθ | A | dσ/dΩ |
|---|---|---|---|---|---|
| -0.50 | 0.24±0.10 | 0.09±0.01 | 0.06 | 0.34±0.04 | 0.19±0.01 |
| -0.46 | 0.26±0.07 | 0.16±0.01 | 0.10 | 0.38±0.03 | 0.28±0.01 |
| -0.42 | 0.24±0.05 | 0.18±0.01 | 0.14 | 0.34±0.02 | 0.39±0.01 |
| -0.38 | 0.22±0.04 | 0.16±0.01 | 0.18 | 0.39±0.02 | 0.53±0.01 |
| -0.34 | 0.10±0.05 | 0.14±0.01 | 0.22 | 0.39±0.02 | 0.68±0.01 |
| -0.30 | 0.12±0.05 | 0.13±0.01 | 0.26 | 0.41±0.02 | 0.87±0.02 |
| -0.26 | 0.06±0.05 | 0.12±0.01 | 0.30 | 0.38±0.01 | 1.12±0.02 |
| -0.22 | 0.01±0.06 | 0.09±0.01 | 0.34 | 0.36±0.01 | 1.32±0.02 |
| -0.18 | -0.12±0.06 | 0.08±0.01 | 0.38 | 0.39±0.01 | 1.70±0.03 |
| -0.14 | 0.03±0.06 | 0.07±0.01 | 0.42 | 0.36±0.01 | 2.09±0.04 |
| -0.10 | 0.17±0.06 | 0.07±0.01 | 0.46 | 0.36±0.01 | 2.38±0.04 |
| -0.06 | 0.25±0.06 | 0.09±0.01 | 0.50 | 0.35±0.01 | 2.49±0.05 |
| -0.02 | 0.27±0.05 | 0.10±0.01 | 0.54 | 0.20±0.04 | |
| 0.02 | 0.26±0.04 | 0.15±0.01 | | | |

Table 3: Momentum in centre of target: 679 MeV/c

| cosθ | A | dσ/dΩ | cosθ | A | dσ/dΩ |
|---|---|---|---|---|---|
| -0.58 | 0.24±0.06 | 0.19±0.01 | 0.02 | 0.10±0.06 | 0.08±0.01 |
| -0.54 | 0.33±0.05 | 0.22±0.01 | 0.06 | 0.23±0.07 | 0.09±0.01 |
| -0.50 | 0.24±0.04 | 0.22±0.01 | 0.10 | 0.41±0.06 | 0.12±0.01 |
| -0.46 | 0.17±0.04 | 0.24±0.01 | 0.14 | 0.38±0.05 | 0.15±0.01 |
| -0.42 | 0.09±0.04 | 0.24±0.01 | 0.18 | 0.42±0.04 | 0.22±0.01 |
| -0.38 | 0.13±0.05 | 0.21±0.01 | 0.22 | 0.41±0.03 | 0.33±0.01 |
| -0.34 | 0.09±0.04 | 0.21±0.01 | 0.26 | 0.43±0.03 | 0.45±0.01 |
| -0.30 | 0.03±0.04 | 0.18±0.01 | 0.30 | 0.34±0.02 | 0.64±0.01 |
| -0.26 | 0.11±0.04 | 0.14±0.01 | 0.34 | 0.37±0.02 | 0.81±0.02 |
| -0.22 | 0.11±0.05 | 0.13±0.01 | 0.38 | 0.36±0.02 | 1.06±0.02 |
| -0.18 | 0.08±0.05 | 0.09±0.01 | 0.42 | 0.32±0.01 | 1.41±0.03 |
| -0.14 | 0.05±0.05 | 0.10±0.01 | 0.46 | 0.33±0.01 | 1.85±0.03 |
| -0.10 | -0.02±0.06 | 0.08±0.01 | 0.50 | 0.31±0.01 | 2.29±0.05 |
| -0.06 | -0.02±0.06 | 0.08±0.01 | 0.54 | 0.30±0.01 | 2.91±0.06 |
| -0.02 | 0.12±0.06 | 0.08±0.01 | 0.58 | 0.30±0.01 | 3.40±0.16 |

Table 4: Momentum in centre of target: 783 MeV/c

| cosθ | A | dσ/dΩ | cosθ | A | dσ/dΩ |
|---|---|---|---|---|---|
| -0.66 | 0.55±0.22 | 0.26±0.05 | 0.02 | 0.00±0.07 | 0.08±0.01 |
| -0.62 | 0.32±0.06 | 0.17±0.01 | 0.06 | 0.14±0.07 | 0.08±0.01 |
| -0.58 | 0.29±0.06 | 0.20±0.01 | 0.10 | 0.25±0.09 | 0.08±0.01 |
| -0.54 | 0.15±0.05 | 0.22±0.01 | 0.14 | 0.32±0.09 | 0.08±0.01 |
| -0.50 | 0.15±0.05 | 0.23±0.01 | 0.18 | 0.36±0.08 | 0.10±0.01 |
| -0.46 | 0.16±0.05 | 0.25±0.01 | 0.22 | 0.45±0.07 | 0.14±0.01 |
| -0.42 | 0.09±0.05 | 0.22±0.01 | 0.26 | 0.42±0.05 | 0.19±0.01 |
| -0.38 | 0.22±0.05 | 0.23±0.01 | 0.30 | 0.43±0.04 | 0.30±0.01 |
| -0.34 | 0.17±0.04 | 0.22±0.01 | 0.34 | 0.38±0.03 | 0.45±0.01 |
| -0.30 | 0.10±0.04 | 0.19±0.01 | 0.38 | 0.34±0.02 | 0.70±0.02 |
| -0.26 | 0.18±0.04 | 0.19±0.01 | 0.42 | 0.34±0.02 | 0.95±0.03 |
| -0.22 | 0.13±0.04 | 0.17±0.01 | 0.46 | 0.30±0.01 | 1.36±0.03 |
| -0.18 | 0.17±0.05 | 0.12±0.01 | 0.50 | 0.32±0.01 | 1.69±0.04 |
| -0.14 | 0.16±0.05 | 0.14±0.01 | 0.54 | 0.29±0.01 | 2.07±0.04 |
| -0.10 | 0.15±0.05 | 0.13±0.01 | 0.58 | 0.28±0.01 | 2.87±0.05 |
| -0.06 | 0.23±0.06 | 0.10±0.01 | 0.62 | 0.28±0.01 | 3.76±0.06 |
| -0.02 | 0.11±0.06 | 0.09±0.01 | 0.66 | 0.22±0.04 | 4.19±0.21 |

Table 5: Momentum in centre of target: 886 MeV/c

| cosθ | A | dσ/dΩ | cosθ | A | dσ/dΩ |
|---|---|---|---|---|---|
| -0.70 | 0.45±0.16 | 0.10±0.01 | 0.02 | 0.26±0.05 | 0.14±0.01 |
| -0.66 | 0.38±0.10 | 0.10±0.01 | 0.06 | 0.21±0.06 | 0.11±0.01 |
| -0.62 | 0.48±0.08 | 0.11±0.01 | 0.10 | 0.19±0.07 | 0.09±0.01 |
| -0.58 | 0.27±0.07 | 0.12±0.01 | 0.14 | 0.32±0.09 | 0.08±0.01 |
| -0.54 | 0.33±0.06 | 0.13±0.01 | 0.18 | 0.28±0.10 | 0.08±0.01 |
| -0.50 | 0.28±0.06 | 0.15±0.01 | 0.22 | 0.24±0.10 | 0.08±0.01 |
| -0.46 | 0.37±0.06 | 0.16±0.01 | 0.26 | 0.38±0.08 | 0.10±0.01 |
| -0.42 | 0.33±0.05 | 0.17±0.01 | 0.30 | 0.50±0.06 | 0.12±0.01 |
| -0.38 | 0.31±0.04 | 0.17±0.01 | 0.34 | 0.39±0.04 | 0.20±0.01 |
| -0.34 | 0.27±0.05 | 0.17±0.01 | 0.38 | 0.35±0.03 | 0.29±0.01 |
| -0.30 | 0.31±0.04 | 0.16±0.01 | 0.42 | 0.40±0.03 | 0.41±0.02 |
| -0.26 | 0.37±0.04 | 0.18±0.01 | 0.46 | 0.36±0.02 | 0.68±0.02 |
| -0.22 | 0.28±0.04 | 0.19±0.01 | 0.50 | 0.34±0.02 | 0.94±0.02 |
| -0.18 | 0.28±0.04 | 0.18±0.01 | 0.54 | 0.30±0.01 | 1.40±0.03 |
| -0.14 | 0.17±0.04 | 0.17±0.01 | 0.58 | 0.28±0.01 | 1.56±0.03 |
| -0.10 | 0.25±0.04 | 0.18±0.01 | 0.62 | 0.26±0.01 | 2.41±0.04 |
| -0.06 | 0.22±0.05 | 0.15±0.01 | 0.66 | 0.17±0.01 | 3.32±0.04 |
| -0.02 | 0.25±0.05 | 0.13±0.01 | 0.70 | 0.20±0.02 | 3.94±0.08 |

Table 6: Momentum in centre of target: 988 MeV/c

| cosθ | A | dσ/dΩ | cosθ | A | dσ/dΩ |
|---|---|---|---|---|---|
| -0.78 | 0.05±0.25 | 0.03±0.01 | -0.02 | 0.31±0.04 | 0.14±0.01 |
| -0.74 | -0.02±0.13 | 0.05±0.01 | 0.02 | 0.29±0.05 | 0.14±0.01 |
| -0.70 | 0.11±0.11 | 0.05±0.01 | 0.06 | 0.31±0.05 | 0.13±0.01 |
| -0.66 | 0.06±0.10 | 0.06±0.01 | 0.10 | 0.26±0.05 | 0.12±0.01 |
| -0.62 | 0.29±0.10 | 0.06±0.01 | 0.14 | 0.26±0.05 | 0.10±0.01 |
| -0.58 | 0.19±0.09 | 0.08±0.01 | 0.18 | 0.31±0.06 | 0.09±0.01 |
| -0.54 | 0.42±0.10 | 0.07±0.01 | 0.22 | 0.25±0.06 | 0.09±0.01 |
| -0.50 | 0.32±0.09 | 0.08±0.01 | 0.26 | 0.31±0.07 | 0.06±0.01 |
| -0.46 | 0.33±0.07 | 0.09±0.01 | 0.30 | 0.31±0.07 | 0.07±0.01 |
| -0.42 | 0.38±0.08 | 0.10±0.01 | 0.34 | 0.36±0.06 | 0.09±0.01 |
| -0.38 | 0.39±0.05 | 0.13±0.01 | 0.38 | 0.44±0.05 | 0.12±0.01 |
| -0.34 | 0.47±0.05 | 0.13±0.01 | 0.42 | 0.46±0.04 | 0.23±0.01 |
| -0.30 | 0.44±0.05 | 0.14±0.01 | 0.46 | 0.46±0.03 | 0.39±0.02 |
| -0.26 | 0.44±0.05 | 0.14±0.01 | 0.50 | 0.39±0.02 | 0.55±0.02 |
| -0.22 | 0.38±0.04 | 0.15±0.01 | 0.54 | 0.36±0.02 | 0.88±0.03 |
| -0.18 | 0.36±0.04 | 0.16±0.01 | 0.58 | 0.35±0.02 | 1.00±0.03 |
| -0.14 | 0.38±0.04 | 0.15±0.01 | 0.62 | 0.33±0.02 | 1.66±0.04 |
| -0.10 | 0.38±0.04 | 0.16±0.01 | 0.66 | 0.29±0.02 | 2.45±0.11 |
| -0.06 | 0.37±0.04 | 0.16±0.01 | 0.70 | 0.25±0.03 | 2.76±0.33 |

Table 7: Momentum in centre of target: 1089 MeV/c

| cosθ | A | dσ/dΩ | cosθ | A | dσ/dΩ |
|---|---|---|---|---|---|
| -0.78 | -0.54±0.17 | 0.05±0.01 | 0.02 | 0.34±0.05 | 0.21±0.01 |
| -0.74 | -0.18±0.16 | 0.04±0.01 | 0.06 | 0.30±0.05 | 0.19±0.01 |
| -0.70 | -0.58±0.17 | 0.04±0.01 | 0.10 | 0.34±0.05 | 0.19±0.01 |
| -0.66 | -0.45±0.17 | 0.05±0.01 | 0.14 | 0.32±0.06 | 0.15±0.01 |
| -0.62 | -0.15±0.21 | 0.04±0.01 | 0.18 | 0.27±0.06 | 0.15±0.01 |
| -0.58 | 0.04±0.20 | 0.05±0.01 | 0.22 | 0.22±0.07 | 0.13±0.01 |
| -0.54 | 0.34±0.16 | 0.05±0.01 | 0.26 | 0.24±0.07 | 0.10±0.01 |
| -0.50 | 0.54±0.15 | 0.06±0.01 | 0.30 | 0.30±0.08 | 0.09±0.01 |
| -0.46 | 0.39±0.13 | 0.07±0.01 | 0.34 | 0.33±0.08 | 0.08±0.01 |
| -0.42 | 0.64±0.11 | 0.10±0.01 | 0.38 | 0.49±0.08 | 0.11±0.01 |
| -0.38 | 0.54±0.10 | 0.11±0.01 | 0.42 | 0.51±0.07 | 0.13±0.01 |
| -0.34 | 0.60±0.08 | 0.11±0.01 | 0.46 | 0.57±0.05 | 0.23±0.02 |
| -0.30 | 0.46±0.07 | 0.14±0.01 | 0.50 | 0.47±0.04 | 0.36±0.02 |
| -0.26 | 0.40±0.06 | 0.15±0.01 | 0.54 | 0.37±0.03 | 0.67±0.03 |
| -0.22 | 0.39±0.06 | 0.15±0.01 | 0.58 | 0.34±0.03 | 0.83±0.03 |
| -0.18 | 0.41±0.05 | 0.22±0.01 | 0.62 | 0.36±0.02 | 1.20±0.04 |
| -0.14 | 0.39±0.05 | 0.19±0.01 | 0.66 | 0.31±0.02 | 1.98±0.05 |
| -0.10 | 0.31±0.05 | 0.19±0.01 | 0.70 | 0.29±0.02 | 2.93±0.06 |
| -0.06 | 0.36±0.05 | 0.19±0.01 | 0.74 | 0.28±0.02 | 4.22±0.07 |
| -0.02 | 0.31±0.05 | 0.19±0.01 | 0.78 | 0.24±0.02 | |

Table 8: Momentum in centre of target: 1190 MeV/c

| cosθ | A | dσ/dΩ | cosθ | A | dσ/dΩ |
|---|---|---|---|---|---|
| -0.82 | -0.55±0.23 | 0.05±0.01 | 0.02 | 0.32±0.03 | 0.19±0.01 |
| -0.78 | -0.39±0.10 | 0.07±0.01 | 0.06 | 0.29±0.03 | 0.21±0.01 |
| -0.74 | -0.34±0.10 | 0.04±0.01 | 0.10 | 0.23±0.03 | 0.22±0.01 |
| -0.70 | -0.25±0.11 | 0.04±0.01 | 0.14 | 0.27±0.03 | 0.21±0.01 |
| -0.66 | -0.15±0.11 | 0.04±0.01 | 0.18 | 0.23±0.03 | 0.20±0.01 |
| -0.62 | -0.30±0.15 | 0.03±0.01 | 0.22 | 0.22±0.03 | 0.20±0.01 |
| -0.58 | 0.05±0.15 | 0.04±0.01 | 0.26 | 0.21±0.03 | 0.16±0.01 |
| -0.54 | 0.17±0.12 | 0.03±0.01 | 0.30 | 0.26±0.04 | 0.15±0.01 |
| -0.50 | 0.63±0.13 | 0.05±0.01 | 0.34 | 0.29±0.04 | 0.13±0.01 |
| -0.46 | 0.53±0.09 | 0.05±0.01 | 0.38 | 0.33±0.05 | 0.11±0.01 |
| -0.42 | 0.45±0.08 | 0.07±0.01 | 0.42 | 0.42±0.05 | 0.12±0.01 |
| -0.38 | 0.58±0.07 | 0.08±0.01 | 0.46 | 0.45±0.05 | 0.14±0.01 |
| -0.34 | 0.64±0.05 | 0.11±0.01 | 0.50 | 0.44±0.03 | 0.23±0.01 |
| -0.30 | 0.52±0.05 | 0.10±0.01 | 0.54 | 0.41±0.03 | 0.32±0.01 |
| -0.26 | 0.56±0.04 | 0.11±0.01 | 0.58 | 0.35±0.02 | 0.53±0.02 |
| -0.22 | 0.50±0.04 | 0.13±0.01 | 0.62 | 0.36±0.02 | 0.83±0.02 |
| -0.18 | 0.47±0.04 | 0.14±0.01 | 0.66 | 0.28±0.02 | 1.36±0.03 |
| -0.14 | 0.41±0.04 | 0.15±0.01 | 0.70 | 0.29±0.02 | 2.33±0.04 |
| -0.10 | 0.34±0.03 | 0.19±0.01 | 0.74 | 0.32±0.04 | 3.59±0.08 |
| -0.06 | 0.40±0.03 | 0.18±0.01 | 0.78 | 0.27±0.03 | |
| -0.02 | 0.38±0.03 | 0.20±0.01 | 0.82 | 0.21±0.03 | |

Table 9: Momentum in centre of target: 1291 MeV/c

| cosθ | A | dσ/dΩ | cosθ | A | dσ/dΩ |
|---|---|---|---|---|---|
| -0.74 | -0.05±0.14 | 0.06±0.01 | 0.06 | 0.27±0.05 | 0.24±0.01 |
| -0.70 | -0.23±0.18 | 0.06±0.01 | 0.10 | 0.37±0.05 | 0.25±0.01 |
| -0.66 | 0.07±0.17 | 0.06±0.01 | 0.14 | 0.30±0.04 | 0.28±0.01 |
| -0.62 | -0.13±0.19 | 0.03±0.01 | 0.18 | 0.33±0.05 | 0.27±0.01 |
| -0.58 | 0.10±0.23 | 0.05±0.01 | 0.22 | 0.24±0.05 | 0.26±0.01 |
| -0.54 | 0.40±0.20 | 0.06±0.01 | 0.26 | 0.29±0.05 | 0.27±0.01 |
| -0.50 | 0.63±0.22 | 0.06±0.01 | 0.30 | 0.36±0.05 | 0.25±0.01 |
| -0.46 | 0.44±0.16 | 0.07±0.01 | 0.34 | 0.30±0.05 | 0.22±0.01 |
| -0.42 | 0.54±0.14 | 0.08±0.01 | 0.38 | 0.24±0.06 | 0.19±0.01 |
| -0.38 | 0.74±0.15 | 0.08±0.01 | 0.42 | 0.45±0.07 | 0.15±0.01 |
| -0.34 | 0.56±0.10 | 0.08±0.01 | 0.46 | 0.41±0.09 | 0.13±0.02 |
| -0.30 | 0.69±0.09 | 0.08±0.01 | 0.50 | 0.63±0.11 | 0.13±0.02 |
| -0.26 | 0.70±0.08 | 0.13±0.01 | 0.54 | 0.61±0.07 | 0.19±0.02 |
| -0.22 | 0.62±0.08 | 0.14±0.02 | 0.58 | 0.55±0.06 | 0.30±0.02 |
| -0.18 | 0.60±0.07 | 0.12±0.01 | 0.62 | 0.45±0.04 | 0.55±0.03 |
| -0.14 | 0.54±0.07 | 0.14±0.01 | 0.66 | 0.44±0.03 | 1.03±0.04 |
| -0.10 | 0.54±0.06 | 0.17±0.01 | 0.70 | 0.36±0.03 | 1.68±0.05 |
| -0.06 | 0.55±0.06 | 0.19±0.01 | 0.74 | 0.29±0.02 | 2.98±0.07 |
| -0.02 | 0.39±0.05 | 0.20±0.01 | 0.78 | 0.27±0.02 | 4.64±0.09 |
| 0.02 | 0.43±0.05 | 0.21±0.01 | 0.82 | 0.23±0.02 | |

Table 10: Momentum in centre of target: 1400 MeV/c

| cosθ | A | dσ/dΩ | cosθ | A | dσ/dΩ |
|---|---|---|---|---|---|
| -0.86 | -0.01±0.19 | 0.05±0.01 | -0.02 | 0.41±0.05 | 0.17±0.01 |
| -0.82 | -0.10±0.13 | 0.04±0.01 | 0.02 | 0.44±0.04 | 0.19±0.01 |
| -0.78 | -0.25±0.11 | 0.07±0.01 | 0.06 | 0.46±0.04 | 0.19±0.01 |
| -0.74 | -0.22±0.11 | 0.06±0.01 | 0.10 | 0.33±0.04 | 0.22±0.01 |
| -0.70 | -0.19±0.13 | 0.05±0.01 | 0.14 | 0.36±0.04 | 0.20±0.01 |
| -0.66 | -0.22±0.13 | 0.05±0.01 | 0.18 | 0.37±0.04 | 0.22±0.01 |
| -0.62 | -0.20±0.17 | 0.04±0.01 | 0.22 | 0.35±0.04 | 0.24±0.01 |
| -0.58 | -0.27±0.17 | 0.04±0.01 | 0.26 | 0.26±0.04 | 0.23±0.01 |
| -0.54 | 0.30±0.15 | 0.03±0.01 | 0.30 | 0.25±0.04 | 0.21±0.01 |
| -0.50 | 0.38±0.14 | 0.04±0.01 | 0.34 | 0.38±0.05 | 0.17±0.01 |
| -0.46 | 0.59±0.12 | 0.07±0.01 | 0.38 | 0.30±0.05 | 0.16±0.01 |
| -0.42 | 0.65±0.13 | 0.05±0.01 | 0.42 | 0.31±0.06 | 0.13±0.01 |
| -0.38 | 0.72±0.12 | 0.06±0.01 | 0.46 | 0.48±0.07 | 0.11±0.01 |
| -0.34 | 0.77±0.10 | 0.09±0.01 | 0.50 | 0.57±0.06 | 0.14±0.01 |
| -0.30 | 0.71±0.09 | 0.07±0.01 | 0.54 | 0.54±0.06 | 0.17±0.02 |
| -0.26 | 0.57±0.07 | 0.09±0.01 | 0.58 | 0.49±0.04 | 0.29±0.02 |
| -0.22 | 0.69±0.06 | 0.09±0.01 | 0.62 | 0.43±0.04 | 0.60±0.03 |
| -0.18 | 0.61±0.06 | 0.11±0.01 | 0.66 | 0.40±0.03 | 1.00±0.03 |
| -0.14 | 0.59±0.06 | 0.10±0.01 | 0.70 | 0.32±0.02 | 1.78±0.05 |
| -0.10 | 0.54±0.05 | 0.12±0.01 | 0.74 | 0.32±0.02 | 3.06±0.06 |
| -0.06 | 0.57±0.06 | 0.13±0.01 | 0.78 | 0.30±0.02 | 4.38±0.09 |

Table 11: Momentum in centre of target: 1416 MeV/c

| cosθ | A | dσ/dΩ | cosθ | A | dσ/dΩ |
|---|---|---|---|---|---|
| -0.78 | 0.26±0.21 | 0.04±0.01 | 0.02 | 0.43±0.06 | 0.20±0.01 |
| -0.74 | -0.27±0.18 | 0.07±0.01 | 0.06 | 0.33±0.06 | 0.20±0.01 |
| -0.70 | -0.37±0.21 | 0.06±0.01 | 0.10 | 0.36±0.06 | 0.24±0.02 |
| -0.66 | 0.09±0.23 | 0.04±0.01 | 0.14 | 0.39±0.06 | 0.24±0.02 |
| -0.62 | -0.67±0.24 | 0.05±0.01 | 0.18 | 0.38±0.06 | 0.22±0.02 |
| -0.58 | 0.19±0.23 | 0.04±0.01 | 0.22 | 0.35±0.06 | 0.28±0.02 |
| -0.54 | 0.22±0.22 | 0.04±0.01 | 0.26 | 0.30±0.06 | 0.31±0.02 |
| -0.50 | 0.51±0.24 | 0.03±0.01 | 0.30 | 0.26±0.06 | 0.24±0.02 |
| -0.46 | 0.70±0.22 | 0.07±0.01 | 0.34 | 0.35±0.06 | 0.23±0.02 |
| -0.42 | 0.73±0.17 | 0.06±0.01 | 0.38 | 0.27±0.07 | 0.24±0.02 |
| -0.38 | 0.83±0.21 | 0.06±0.01 | 0.42 | 0.34±0.08 | 0.15±0.01 |
| -0.34 | 0.59±0.13 | 0.10±0.02 | 0.46 | 0.39±0.09 | 0.14±0.01 |
| -0.30 | 0.45±0.11 | 0.07±0.01 | 0.50 | 0.46±0.10 | 0.10±0.02 |
| -0.26 | 0.55±0.10 | 0.14±0.02 | 0.54 | 0.58±0.08 | 0.19±0.02 |
| -0.22 | 0.76±0.10 | 0.12±0.02 | 0.58 | 0.55±0.06 | 0.27±0.03 |
| -0.18 | 0.48±0.09 | 0.10±0.01 | 0.62 | 0.38±0.05 | 0.56±0.04 |
| -0.14 | 0.49±0.08 | 0.14±0.01 | 0.66 | 0.29±0.04 | 0.95±0.06 |
| -0.10 | 0.51±0.08 | 0.15±0.01 | 0.70 | 0.33±0.04 | 1.53±0.10 |
| -0.06 | 0.45±0.08 | 0.15±0.01 | 0.74 | 0.32±0.02 | 3.04±0.39 |
| -0.02 | 0.41±0.07 | 0.21±0.01 | 0.78 | 0.27±0.02 | 4.76±0.60 |

Table 12: Momentum in centre of target: 1449 MeV/c

| cosθ | A | dσ/dΩ | cosθ | A | dσ/dΩ |
|---|---|---|---|---|---|
| -0.86 | 0.06±0.16 | 0.07±0.01 | -0.02 | 0.52±0.06 | 0.13±0.01 |
| -0.82 | 0.24±0.13 | 0.07±0.01 | 0.02 | 0.44±0.06 | 0.16±0.01 |
| -0.78 | -0.03±0.15 | 0.06±0.01 | 0.06 | 0.41±0.06 | 0.17±0.01 |
| -0.74 | -0.18±0.15 | 0.04±0.01 | 0.10 | 0.44±0.05 | 0.18±0.01 |
| -0.70 | -0.34±0.15 | 0.06±0.01 | 0.14 | 0.33±0.05 | 0.18±0.01 |
| -0.66 | -0.28±0.18 | 0.04±0.01 | 0.18 | 0.38±0.05 | 0.19±0.01 |
| -0.62 | -0.04±0.20 | 0.04±0.01 | 0.22 | 0.30±0.05 | 0.23±0.01 |
| -0.58 | -0.04±0.16 | 0.05±0.01 | 0.26 | 0.27±0.05 | 0.21±0.01 |
| -0.54 | -0.09±0.18 | 0.04±0.01 | 0.30 | 0.28±0.05 | 0.22±0.01 |
| -0.50 | 0.47±0.18 | 0.03±0.01 | 0.34 | 0.27±0.05 | 0.18±0.01 |
| -0.46 | 0.39±0.15 | 0.04±0.01 | 0.38 | 0.29±0.06 | 0.15±0.01 |
| -0.42 | 0.60±0.14 | 0.04±0.01 | 0.42 | 0.41±0.08 | 0.10±0.01 |
| -0.38 | 0.46±0.13 | 0.04±0.01 | 0.46 | 0.30±0.08 | 0.11±0.01 |
| -0.34 | 0.55±0.12 | 0.04±0.01 | 0.50 | 0.37±0.08 | 0.12±0.01 |
| -0.30 | 0.75±0.12 | 0.06±0.01 | 0.54 | 0.68±0.08 | 0.13±0.01 |
| -0.26 | 0.65±0.09 | 0.07±0.01 | 0.58 | 0.45±0.06 | 0.25±0.02 |
| -0.22 | 0.55±0.09 | 0.08±0.01 | 0.62 | 0.55±0.05 | 0.38±0.02 |
| -0.18 | 0.66±0.09 | 0.08±0.01 | 0.66 | 0.43±0.04 | 0.75±0.03 |
| -0.14 | 0.64±0.08 | 0.09±0.01 | 0.70 | 0.34±0.03 | 1.29±0.04 |
| -0.10 | 0.50±0.07 | 0.10±0.01 | 0.74 | 0.30±0.02 | 2.37±0.05 |
| -0.06 | 0.48±0.07 | 0.12±0.01 | 0.78 | 0.28±0.02 | 3.75±0.07 |

Table 13: Momentum in centre of target: 1467 MeV/c

| cosθ | A | dσ/dΩ | cosθ | A | dσ/dΩ |
|---|---|---|---|---|---|
| -0.86 | 0.50±0.19 | 0.03±0.01 | -0.02 | 0.46±0.06 | 0.12±0.01 |
| -0.82 | 0.04±0.15 | 0.05±0.01 | 0.02 | 0.44±0.06 | 0.13±0.01 |
| -0.78 | -0.01±0.14 | 0.05±0.01 | 0.06 | 0.53±0.06 | 0.14±0.01 |
| -0.74 | -0.26±0.15 | 0.04±0.01 | 0.10 | 0.37±0.05 | 0.15±0.01 |
| -0.70 | 0.00±0.16 | 0.03±0.01 | 0.14 | 0.37±0.05 | 0.17±0.01 |
| -0.66 | -0.02±0.18 | 0.04±0.01 | 0.18 | 0.31±0.05 | 0.17±0.01 |
| -0.62 | -0.20±0.20 | 0.04±0.01 | 0.22 | 0.28±0.05 | 0.20±0.01 |
| -0.58 | 0.30±0.25 | 0.02±0.01 | 0.26 | 0.33±0.05 | 0.18±0.01 |
| -0.54 | 0.16±0.18 | 0.03±0.01 | 0.30 | 0.32±0.05 | 0.18±0.01 |
| -0.50 | 0.36±0.17 | 0.04±0.01 | 0.34 | 0.28±0.05 | 0.16±0.01 |
| -0.46 | 0.27±0.16 | 0.03±0.01 | 0.38 | 0.31±0.05 | 0.17±0.01 |
| -0.42 | 0.31±0.14 | 0.04±0.01 | 0.42 | 0.29±0.07 | 0.12±0.01 |
| -0.38 | 0.34±0.13 | 0.03±0.01 | 0.46 | 0.31±0.07 | 0.11±0.01 |
| -0.34 | 0.71±0.15 | 0.04±0.01 | 0.50 | 0.47±0.08 | 0.07±0.01 |
| -0.30 | 0.58±0.10 | 0.05±0.01 | 0.54 | 0.48±0.08 | 0.10±0.01 |
| -0.26 | 0.65±0.10 | 0.05±0.01 | 0.58 | 0.45±0.06 | 0.18±0.01 |
| -0.22 | 0.60±0.09 | 0.06±0.01 | 0.62 | 0.45±0.05 | 0.26±0.02 |
| -0.18 | 0.54±0.08 | 0.05±0.01 | 0.66 | 0.46±0.05 | 0.54±0.03 |
| -0.14 | 0.55±0.08 | 0.08±0.01 | 0.70 | 0.36±0.03 | 0.94±0.03 |
| -0.10 | 0.36±0.07 | 0.09±0.01 | 0.74 | 0.35±0.02 | 1.75±0.04 |
| -0.06 | 0.50±0.07 | 0.09±0.01 | 0.78 | 0.34±0.02 | 3.08±0.06 |

Table 14: Momentum in centre of target: 1501 MeV/c

| cosθ | A | dσ/dΩ | cosθ | A | dσ/dΩ |
|---|---|---|---|---|---|
| -0.78 | -0.27±0.17 | 0.08±0.01 | 0.02 | 0.49±0.07 | 0.16±0.01 |
| -0.74 | -0.15±0.17 | 0.07±0.01 | 0.06 | 0.48±0.06 | 0.17±0.01 |
| -0.70 | 0.02±0.19 | 0.04±0.01 | 0.10 | 0.50±0.06 | 0.21±0.01 |
| -0.66 | -0.01±0.21 | 0.03±0.01 | 0.14 | 0.40±0.06 | 0.22±0.01 |
| -0.62 | -0.05±0.19 | 0.05±0.01 | 0.18 | 0.38±0.05 | 0.23±0.01 |
| -0.58 | 0.31±0.23 | 0.03±0.01 | 0.22 | 0.33±0.05 | 0.25±0.01 |
| -0.54 | 0.30±0.18 | 0.04±0.01 | 0.26 | 0.30±0.05 | 0.25±0.01 |
| -0.50 | 0.16±0.18 | 0.04±0.01 | 0.30 | 0.26±0.05 | 0.27±0.01 |
| -0.46 | 0.29±0.19 | 0.05±0.01 | 0.34 | 0.21±0.05 | 0.27±0.01 |
| -0.42 | 0.44±0.19 | 0.05±0.01 | 0.38 | 0.20±0.05 | 0.21±0.01 |
| -0.38 | 0.56±0.18 | 0.04±0.01 | 0.42 | 0.10±0.06 | 0.19±0.01 |
| -0.34 | 0.61±0.16 | 0.05±0.01 | 0.46 | 0.08±0.07 | 0.14±0.01 |
| -0.30 | 0.45±0.11 | 0.07±0.01 | 0.50 | 0.19±0.08 | 0.10±0.01 |
| -0.26 | 0.58±0.12 | 0.08±0.01 | 0.54 | 0.47±0.09 | 0.13±0.02 |
| -0.22 | 0.46±0.11 | 0.06±0.01 | 0.58 | 0.59±0.08 | 0.15±0.02 |
| -0.18 | 0.52±0.10 | 0.10±0.01 | 0.62 | 0.54±0.07 | 0.26±0.02 |
| -0.14 | 0.47±0.09 | 0.09±0.01 | 0.66 | 0.51±0.07 | 0.40±0.03 |
| -0.10 | 0.60±0.09 | 0.10±0.01 | 0.70 | 0.45±0.05 | 0.84±0.04 |
| -0.06 | 0.48±0.07 | 0.13±0.01 | 0.74 | 0.34±0.03 | 1.58±0.05 |
| -0.02 | 0.43±0.07 | 0.14±0.01 | 0.78 | 0.28±0.02 | 3.03±0.07 |

Table 15: Momentum in centre of target: 1550 MeV/c

## APPENDIX B

Legendre expansion coefficients

Values of Legendre expansion coefficients $a_i/a_0$ and $b_i/a_0$. Expansions are terminated at orders corresponding to the minimum value of $\chi^2/DF$. The errors shown correspond to the diagonal elements of the covariance matrix. The fits are performed using the constraints described in chapter 4.

| p | $a_1/a_0$ | $a_2/a_0$ | $a_3/a_0$ | $a_4/a_0$ | $a_5/a_0$ |
|---|---|---|---|---|---|
| 679 | 2.57±0.08 | 2.58±0.10 | 2.07±0.10 | 1.10±0.06 | 0.45±0.02 |
| 783 | 2.56±0.07 | 2.82±0.10 | 2.46±0.10 | 1.47±0.07 | 0.77±0.04 |
| 886 | 2.47±0.09 | 3.02±0.13 | 2.71±0.13 | 1.85±0.10 | 1.15±0.06 |
| 988 | 2.24±0.09 | 3.32±0.17 | 2.73±0.16 | 2.55±0.17 | 1.32±0.09 |
| 1089 | 2.82±0.09 | 3.41±0.14 | 3.81±0.18 | 2.73±0.15 | 2.21±0.12 |
| 1190 | 2.71±0.08 | 3.50±0.12 | 3.78±0.15 | 3.06±0.14 | 2.32±0.11 |
| 1291 | 2.66±0.09 | 3.61±0.15 | 3.86±0.19 | 3.39±0.19 | 2.55±0.14 |
| 1400 | 2.63±0.06 | 3.68±0.10 | 3.95±0.12 | 3.74±0.13 | 2.84±0.10 |
| 1416 | 2.56±0.07 | 3.72±0.13 | 3.84±0.16 | 3.79±0.18 | 2.77±0.13 |
| 1449 | 2.56±0.08 | 3.71±0.14 | 3.83±0.16 | 3.77±0.18 | 2.73±0.13 |
| 1467 | 2.70±0.07 | 3.79±0.12 | 4.21±0.16 | 3.95±0.17 | 3.26±0.14 |
| 1501 | 2.74±0.07 | 3.87±0.12 | 4.39±0.16 | 4.20±0.17 | 3.58±0.15 |
| 1550 | 3.07±0.07 | 3.80±0.10 | 5.00±0.16 | 4.10±0.15 | 4.22±0.15 |

Table 16: Legendre expansion coefficients ($a_i/a_0$)

| p | $b_1/a_0$ | $b_2/a_0$ | $b_3/a_0$ | $b_4/a_0$ | $b_5/a_0$ |
|---|---|---|---|---|---|
| 679 | .075±.007 | .160±.019 | -.006±.001 | .049±.008 | -.060±.009 |
| 783 | .181±.016 | .301±.031 | .184±.022 | .221±.030 | .067±.009 |
| 886 | .089±.009 | .134±.017 | .060±.009 | .073±.012 | -.015±.003 |
| 988 | .050±.006 | .031±.005 | .026±.005 | -.003±.001 | -.012±.002 |
| 1089 | .080±.008 | .085±.010 | .073±.010 | .053±.009 | .024±.004 |
| 1190 | .103±.009 | .147±.015 | .114±.014 | .130±.018 | .061±.008 |
| 1291 | .051±.005 | .055±.007 | .038±.006 | .036±.006 | .011±.002 |
| 1400 | .084±.006 | .087±.007 | .079±.007 | .066±.007 | .042±.004 |
| 1416 | .084±.007 | .092±.010 | .087±.011 | .072±.010 | .050±.007 |
| 1449 | .070±.006 | .065±.007 | .062±.008 | .040±.006 | .029±.004 |
| 1467 | .055±.004 | .061±.006 | .043±.005 | .039±.005 | .010±.001 |
| 1501 | .060±.005 | .067±.006 | .058±.006 | .048±.006 | .025±.003 |
| 1550 | .054±.004 | .057±.005 | .043±.004 | .041±.004 | .022±.002 |

Table 17: Legendre expansion coefficients ($b_i/a_0$)